Complex multicomponent real-fluid thermodynamic model for high-pressure Diesel fuel injection

C. Rodriguez [a,*], Houman B. Rokni [a,b], P. Koukouvinis [a], Ashutosh Gupta [c], M. Gavaises [a]

[a] *School of Mathematics, Computer Science & Engineering, Department of Mechanical Engineering & Aeronautics, City University London, Northampton Square EC1V 0HB, United Kingdom*

[b] *Afton Chemical Ltd., Bracknell, Berkshire RG12 2UW, UK*

[c] *Afton Chemical Corp., Richmond, VA 23219, USA*

**Corresponding author: Carlos.Rodriguez@city.ac.uk*

Abstract

The Perturbed-Chain Statistical Associating Fluid Theory (PC-SAFT) has been coupled with Vapor-Liquid Equilibrium (VLE) calculations in a density-based solver of the Navier-Stokes equations to perform multicomponent two-phase simulations of Diesel injections at high-pressure conditions. This molecular-based EoS requires three empirically determined but well-known parameters to model the properties of a specific component, and thus, there is no need for extensive model calibration, as is typically the case when the NIST (REFPROP) library is utilised. PC-SAFT can handle flexibly the thermodynamic properties of multi-component mixtures for which the NIST (REFPROP) library supports only limited component combinations. Moreover, complex hydrocarbon mixtures can be modelled as a single pseudo-component knowing its number averaged molecular weight (MW) and hydrogen-to-carbon (HN/CN) ratio. Published molecular dynamic simulations have been utilised to demonstrate that the developed algorithm properly captures the VLE interface at high-pressure conditions. Several advection test cases and shock tube problems were performed to validate the numerical framework using analytical and exact solutions. Additionally, two-dimensional simulations of n-dodecane and Diesel injections into nitrogen are included to demonstrate the multidimensional, multispecies and multiphase capability of the numerical framework.

Keywords: Subcritical, PC-SAFT EoS, Diesel Fuel Injection

Nomenclature

List of abbreviations

AAD	Average Absolute Deviation
CFD	Computational Fluid Dynamics
CFL	Courant–Friedrichs–Lewy
CPA	Cubic Plus Association
ECN	Engine Combustion Network
ENO	Essentially Non-Oscillatory
EoS	Equation of State
FC	Fully Conservative
GC	Group Contribution

HLLC	Harten-Lax-van Leer-Contact
HN/CN	Hydrogen-to-Carbon Ratio
LES	Large Eddy Simulation
MW	Number Averaged Molecular Weight
N-S	Navier-Stokes
PNAs	Poly-Nuclear Aromatics
PR	Peng-Robinson
PC-SAFT	Perturbed Chain Statistical Associating Fluid Theory
QC	Quasi-Conservative
RK2	Second-order Runge–Kutta
SAFT-BACK	Boublik-Alder-Chen-Kreglewshi
SRK	Soave-Redlich-Kwong
SSP-RK3	Third-order strong-stability-preserving Runge–Kutta
TPn flash	Isothermal-Isobaric Flash
TVD	Total Variation Diminishing
TPD	Tangent Plane Distance
VLE	Vapor-Liquid Equilibrium
WENO	Weighted Essentially Non-Oscillatory

List of Symbols

$\tilde{a}^{res}$	Reduced Helmholtz free energy [-]
c	Sound speed [m s^{-1}]
d	Temperature-dependent segment diameter [Å]
e	Internal energy [J mol^{-1}]
h	Enthalpy [J mol^{-1}]
g	Gibbs energy [J mol^{-1}]
I	Integrals of the perturbation theory [-]
k_b	Boltzmann constant [J K^{-1}]
m	Number of segments per chain [-]
$\bar{m}$	Mean segment number in the system [-]
M_M	Molecular weight [g/mol]
N_A	Avogadro's number [mol^{-1}]
p	Pressure [Pa]
p_c	Critical pressure [Pa]
R	Gas constant [J mol^{-1} K^{-1}]
T	Temperature [K]
T_c	Critical temperature [K]
x_i	Mole fraction of component i [-]
w	Acentric factor [-]
Z	Compressibility factor [-]

Greek Letters

β	Overall fraction of vapour phase [-]
ε	Depth of pair potential [J]
η	Packing fraction [-]
ρ	Density [kg/m^3]
ρ_m	Total number density of molecules [1/Å^3]

σ_d Segment diameter [Å]
θ Vapour volume fraction [-]
φ Fugacity coefficient [-]
μ Chemical potential [J mol^{-1}]

Superscripts
EQ Equilibrium
$disp$ Contribution due to dispersive attraction
hc Residual contribution of hard-chain system
hs Residual contribution of hard-sphere system
id Ideal gas contribution

1. Introduction

This research is focused on improving the thermodynamic models employed to simulate fuel mixing at elevated pressures. To correctly model the combustion in Diesel engines one needs to characterise the atomisation and mixing of sprays. However, even nowadays these processes are not completely understood. According to the experiments performed by several authors [1]–[5], supercritical mixing exists at pressures near or slightly higher than the critical pressure of the liquid fuel. [6], [7] stated that the convection-diffusion phenomena described by the Navier-Stokes equations governs Diesel engine conditions. More recently, in [8] it was determined that the surface tension remains in effect at the gas–liquid interfaces in ambient conditions slightly above the critical point of the fuel. However, at higher pressure and temperature conditions the surface tension diminishes, as expected for supercritical fuel–air mixtures. Diesel engine operation conditions are considered to be in the diffused controlled mixing regime. In a following study [9], the authors carried out systematic measurements using high-speed long-distance microscopy for three single-component fuels (n-heptane, n-dodecane, n-hexadecane) injected into gas (89.71% N_2, 6.52% CO_2 and 3.77% H_2O) at elevated temperatures (700–1200 K) and pressures (2–11 MPa). The classical evaporation/diffusive mixing boundaries were moved towards higher pressures and temperatures placing Diesel engines conditions in the classical evaporation regime. In [10] the evaporation of n-alkane fuels into nitrogen was investigated at different pressure and temperature conditions carrying out molecular dynamic simulations. The aim of this work was to understand how the transition from classical two-phase evaporation to one- phase diffusion-controlled mixing takes place. Two regimes are identified: (1) subcritical evaporation where a distinctive interface exists separating the liquid core and the ambient gases; and (2) supercritical evaporation where initially the liquid has a surface tension that decreases rapidly and vanishes. In the supercritical evaporation regime, the evaporation rate increases and reaches a maximum after which there is a transition to the supercritical stage. The results obtained have a high degree of agreement against the experimental results obtained by [9].

Numerous simulations of Diesel sprays in the literature exist, which employ Lagrangian methods considering a sharp gas-liquid interface which evolve according to primary and secondary breakup models and evaporation [11]–[13]. However, this configuration presents some limitations to accurately capture dense flow regimes near the nozzle where the liquid fuels disintegrate into ligaments that then form droplets. Moreover, they are sensitive to calibration parameters. In [14], [15] an Eulerian density-based methodology was used to model the primary atomisation of the injected liquid accounting for compressibility effects associated with the high-pressure and injection velocity. A single-phase dense-gas approach was combined

with the Peng-Robinson (PR) EoS. However, n-dodecane/nitrogen mixtures are a TYPE IV mixture, which means that the critical temperature of the mixture is higher than the lower critical temperature of the components and lower than then the higher critical temperature of the compounds. On the other hand, the critical pressure is higher than the critical pressure of the components. Considering that the pressures that can be found in the combustion chamber of Diesel engines are lower than the critical pressure of some nitrogen/fuel mixtures, the VLE state must be included in the simulation. In [16], [17] a multi-species two-phase model for Eulerian large-eddy simulations (LES) was developed. A thermodynamic solver that can compute the properties of a homogenous mixture in supercritical or subcritical states was employed. The LES including VLE thermodynamics of the so-called Spray A benchmark case of the Engine Combustion Network (ECN) performed by [16] shows a high degree of agreement against the available experimental data. Although according to [9], [10] the Spray A ambient conditions (900K, 6MPa) fall in the classic evaporation regime, the authors of [16] justified the use of a diffuse interface due to the high Weber number and low Stokes number. The authors pointed out the issues of employing cubic EoS for modelling hydrocarbon properties at temperatures found inside the injection system [18]–[20]. In [16], due to the 8.6% error when compared to NIST (REFPROP) in the density prediction of n-dodecane at 363K, it was necessary to increase the injection velocity to match the mass-flow measurement leading to an error in the predicted velocity of 50 m/s. These problems could be overcome by applying SAFT models.

The SAFT EoS is based on the perturbation theory, as extensively studied in [21]–[24]. This EoS was developed by [25], [26] applying Wertheim's theory and extending it to mixtures. Each molecule of the mixture is decomposed into spherical segments of equal size forming a repulsive, hard sphere reference fluid. The attractive interactions between segments are included in the model as well as the segment-segment energy needed to form a chain between the hard-sphere fluid segments. If the segments exhibit associative interactions such as hydrogen bonding, a term for this interaction is also included. Among the different variants of the SAFT model, the PC-SAFT is the one implemented here. In this model, hard chains are used as the reference fluid instead of hard spheres. While the SAFT EoS computes segment-segment attractive interactions, the PC-SAFT EoS computes chain-chain interactions, which improves the thermodynamic description of chain-like, fluid mixtures [27]. This molecular-based EoS only requires three empirically determined parameters (when the association term is neglected) to model the properties of a specific component without the need for extensive model calibration. Several publications have highlighted the advantages of the SAFT variants with respect to cubic EoS. [28] shows how the PC-SAFT model presents better results than cubic EoS predicting gas phase compressibility factors and oil phase compressibility. For example, Average Absolute Deviation (AAD) of the gas compressibility factors in the range P=0-1000 bar and T= 0-250 °C for nC_6 are 0.0144 for PC-SAFT, 0.0479 for SRK (applying the Peneloux volume correction) and 0.0425 for PR (applying the Peneloux volume correction). For nC_5, they are 0.0127, 0.0529 and 0.0296 respectively. [29] indicated that the PC-SAFT EoS shows a superior performance to the Cubic Plus Association (CPA) EoS in correlating second order derivative properties, such as speed of sound, dP/dV and dP/dT derivatives, heat capacities and the Joule–Thomson coefficient in the alkanes investigated. The CPA model presents a diverging behaviour in the speed of sound attributed to the wrong description of the dP/dV derivative. Similarly, [30] points out the superiority of the SAFT-BACK (Boublik-Alder-Chen-Kreglewshi) model over the PR EOS. The SAFT-BACK EoS shows reasonable results for the speed of sound in the vapor and liquid phases (AAD% = 2.3%, 2.1%, and 1.8% for methane, ethane, and propane, respectively). However, the results obtained by PR EOS are only similar

to measured data at low pressure conditions. The predicted values at high density ranges present an AAD% for methane, ethane, and propane of 28.6%, 14.7%, and 61.2%, respectively. Moreover, in [31] it was shown how cubic EoS predict a linear increase of the Z factor (compressibility factor) with pressure, while the PC-SAFT EoS presents pressure dependence.

In [19], the PC-SAFT was used to close the Navier-Stokes equations using both a conservative and a quasi-conservative formulation, where the double flux model of [32]–[34] was applied. It was observed how the conservative formulation generates spurious pressure oscillations while the quasi-conservative scheme presents an error in the energy conservation that produce an unphysical quick heat-up of the fuel. In [18], supercritical injections of Diesel fuel modelled as surrogates comprising four, five, eight and nine components were performed taking advantage of the capacity of the PC-SAFT EoS to flexibly handle the thermodynamic properties of multi-component mixtures. Simulations at affordable CPU times were carried out by reducing the number of times the PC-SAFT EoS is solved by computing the pressure and sonic fluid velocity in the cell centres and performing a reconstruction of these variables at each cell face. This technique was found to smooth-out the spurious pressure oscillations associated with conservative schemes when used along with real-fluid EoS. The novelty in this paper is to present a numerical framework that combines PC-SAFT and VLE calculations in a density-based, fully conservative solver of the Navier-Stokes and energy conservation equations. VLE calculations allow to perform simulations where the fuel enters the combustion chamber at low temperatures (subcritical injections). Published molecular dynamic simulations have been employed to demonstrate that the algorithm properly captures the multicomponent VLE interface at high-pressure conditions. A purely predictive method that employs the PC-SAFT EoS for developing pseudo-components, which are defined to replicate the properties of complex hydrocarbon mixtures (e.g., diesel fuels), has been completed and validated to be used in CFD simulations. Then, complex hydrocarbon mixtures can be modelled as a single pseudo-component knowing its MW and HN/CN ratio. Advection test cases and shock tube problems were performed to validate the numerical framework. Two-dimensional simulations of planar Diesel jets are performed to demonstrate the capability of the developed methodology to model subcritical mixing at high-pressure conditions.

2. PC-SAFT Theory and Methodology

In this section it is explained the numerical methodology employed to couple the Navier-Stokes equations, total energy equation, VLE calculations and PC-SAFT model in the same numerical framework. The results of the molecular model and VLE calculations were validated using the experimental results of [45], see Figure 1.

2.a. CFD code

The Navier-Stokes equations for a non-reacting multi-component mixture containing N species in a x-y 2D Cartesian system have been solved employing the finite volume method. Operator splitting as described in [35] is utilised to separate the hyperbolic and parabolic operators. The global time step is computed using the CFL (Courant-Friedrichs-Lewy) criterion of the hyperbolic part. A thermodynamic solver inspired by the work of [16] is employed to approximate the mixture thermophysical properties by performing PC-SAFT and VLE calculations. To compute the convective fluxes: the conservative variables, pressure and speed of sound are interpolated at the cell faces from cell centres using a fifth-order WENO (Weighted Essentially Non-Oscillatory) scheme [18]; the multicomponent HLLC (Harten-Lax-van Leer-Contact) solver is applied to solve the Riemann problem [36]; and the temporal integration is

carried out using a second-order Runge–Kutta (RK2) method applying the filter presented in [18]. In the parabolic sub-step, linear interpolation is performed for computing the conservative variables, temperature and enthalpy on the cell faces from the corresponding values at the cell centres. The model developed by [37] is used to calculate the dynamic viscosity and the thermal conductivity. Figure 2 shows a schematic representation of the CFD code. See Appendix 1.

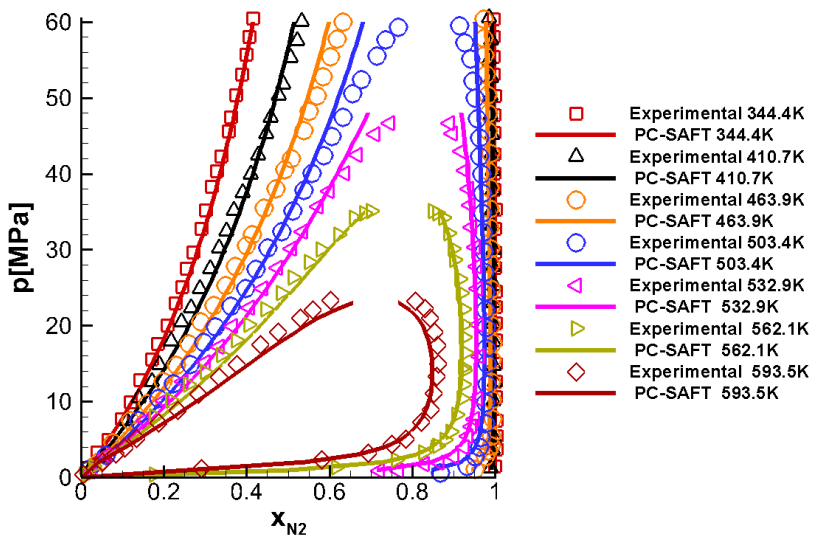

Figure 1. Experimental [38] **and calculated pressure-composition phase diagram for the N_2 (1) + $C_{12}H_{26}$ (2) system. Solid lines: PC-SAFT EoS with kij = 0.144**

- CFD CODE
  - COMPUTE TIME STEP
  - HYPERBOLIC OPERATOR
    - RkStage
      - Set Boundary Conditions
      - Calculate Fluxes
      - *Update*
        - Case (RkStage = 1)
        - $\mathbf{U}^{(1)} = \mathbf{U}^n + \Delta t H_{xy}(\mathbf{U}^n)$,
        - Thermodynamic solver (pressure, sonic fluid velocity, temperature and enthalpy)
        - Case (RkStage=2)
        - $\mathbf{U}^{n+1} = \frac{1}{2}\mathbf{U}^n + \frac{1}{2}\left[\mathbf{U}^{(1)} + \Delta t H_{xy}(\mathbf{U}^{(1)})\right]$
        - Thermodynamic solver (pressure, sonic fluid velocity, temperature and enthalpy)
  - PARABOLIC OPERATOR
    - Set Boundary Conditions
    - Calculate Fluxes
    - Update cell center values
    - Thermodynamic solver (pressure, sonic fluid velocity, temperature and enthalpy)

Figure 2. Schematic representation of the CFD code

2.b. Diesel modelling

Two approximations have been considered to model the properties of Diesel.

Multicomponent Diesel surrogates

In [39] four Diesel surrogates have been proposed, divided into two types depending how close their composition is to real Diesel. The V0A and V0B are two low-accuracy surrogates while V1 and V2 are the two higher-accuracy surrogates. Their molar composition is summarized in Table 1. As pointed out in [40], the PC-SAFT EoS shows the highest degree of agreement with the experimental values in comparison with the results obtained using the model developed at NIST [39], see Table 2.

Pseudo-component method

In [41] was developed a technique that defines a single pseudo-component to represent the compounds found in a hydrocarbon mixture. It only requires two mixture properties as inputs, the MW and HN/CN ratio. Here we briefly describe how to achieve the pseudo-component PC-SAFT parameters needed in this study. The group contribution (GC) parameters of [42] are used to develop the correlations shown in Table 4 for n-alkanes and poly-nuclear aromatics (PNAs) that numerically bound the pseudo-component PC-SAFT parameter values. An averaging parameter, Z, is used to calculate the pseudo-component parameters using Eqs. 1-3. Eqs 4-7 show that Z is calculated using the mixture MW and HN/CN ratio, which can be directly calculated knowing the mixture components or can be obtained using elemental analysis for unknown mixtures. Considering that the PC-SAFT is implemented using loops that depend on the number of components solved, this method allows us to model complex hydrocarbon mixtures as one component, thus, reducing significantly the computational requirements of the simulation but with increasing its accuracy.

Table 1. PC-SAFT pure component parameters [40], [42]

Compound	m	σ (Å)	$\varepsilon/_k$ (K)
n-hexadecane	6.669	3.944	253.59
n-octadecane	7.438	3.948	254.90
n-eicosane	8.207	3.952	255.96
heptamethylnonane	5.603	4.164	266.46
2-methylheptadecane	7.374	3.959	254.83
n-butylcyclohexane	3.682	4.036	282.41
1,3,5-triisopropylcyclohexane	4.959	4.177	297.48
trans-decalin	3.291	4.067	307.98
perhydrophenanthrene	4.211	3.851	337.52
1,2,4-trimethylbenzene	3.610	3.749	284.25
1,3,5-triisopropylbenzene	5.178	4.029	296.68
tetralin	3.088	3.996	337.46
1-methylnaphthalene	3.422	3.901	337.14

Table 2 Comparison between experimentally measured surrogate densities (kg/m^3) at 293.15 K and 0.1 MPa with the NIST and PC-SAFT predictions

Surrogate	Experiment[39]	NIST	PC-SAFT
V0A	818.0	809.1	814.9
V0B	837.5	821.6	833.2
V1	828.4	814.1	825.2
V2	853.0	839.9	861.8

The methodology developed by [41] was validated for modelling density, isothermal compressibility and volumetric thermal expansion coefficient of hydrocarbon mixtures, jet and diesel fuels. However, the pseudo-component must correctly model the internal energy (employed in the conservation of the total energy equation) speed of sound (used to calculate the hyperbolic fluxes and time step), enthalpy (employed in the parabolic operator of the Navier-Stokes equations) and fugacity coefficients (to perform VLE calculations). Using the PC-SAFT, the internal energy, enthalpy and heat capacities at constant pressure and volume (needed to compute the speed of sound) are computed as the sum of ideal and residual contributions. The PC-SAFT pure component parameters obtained employing the method of [41] are used to calculate the residual contributions. The ideal enthalpy of each component is calculated by integrating the ideal heat capacity at constant pressure with respect to temperature [43]. The molar composition of the mixture is used to calculate the ideal enthalpy of the mixture. The ideal internal energy of the mixture is computed employing the ideal enthalpy of the mixture. The ideal heat capacities at constant pressure of each component is computed employing the correlations published in [43]; then, molar fractions are used to compute the ideal heat capacity at constant pressure of the mixture, which is employed to calculate the ideal heat capacity at constant volume.

Table 3. Molar composition for the four Diesel fuel surrogates (V0A, V0B, V1, V2) [39]

Compound	V0A	V0B	V1	V2
n-hexadecane	27.8	-	2.70	-
n-octadecane	-	23.5	20.2	10.8
n-eicosane	-	-	-	0.80
heptamethylnonane	36.3	27.0	29.2	-
2-methylheptadecane	-	-	-	7.3
n-butylcyclohexane	-	-	5.10	19.1
triisopropylcyclohexane	-	-	-	11.0
trans-decalin	14.8	-	5.50	-
perhydrophenanthrene	-	-	-	6.00
1,2,4-trimethylbenzene	-	12.5	7.5	-
1,3,5-triisopropylbenzene	-	-	-	14.7
tetralin	-	20.9	15.4	16.4
1-methylnaphthalene	21.1	16.1	14.4	13.9

$$m_{\text{pseudo}-\text{component}} = (1-Z)m_{\text{n}-\text{alkane}} + Zm_{\text{PNA}} \tag{1}$$

$$(m\sigma)_{\text{pseudo}-\text{component}} = (1-Z)(m\sigma)_{\text{n}-\text{alkane}} + Z(m\sigma)_{PNA} \tag{2}$$

$$\left({}^{\varepsilon}/_{k}\right)_{\text{pseudo}-\text{component}} = (1-Z)\left({}^{\varepsilon}/_{k}\right)_{\text{n}-\text{alkane}} + Z\left({}^{\varepsilon}/_{k}\right)_{\text{PNA}} \tag{3}$$

$$Z = \begin{cases} \frac{\text{DoU}_{\text{mixture}}}{\text{DoU}_{\text{PNA}}}, & \text{MW}_{\text{mixture}} < 178\ \text{g/mol} \\ \frac{\text{DoU}_{\text{mixture}}}{10}, & \text{MW}_{\text{mixture}} \geq 178\ \text{g/mol} \end{cases} \tag{4}$$

$$\text{DoU}_{\text{PNA}} = 0.05993 \times \text{MW} - 0.68158 \tag{5}$$

$$\mathrm{CN_{mixture}} = \frac{\mathrm{MW_{mixture}}}{12.01+1.01\left((\mathrm{HN/CN})_{\mathrm{mixture}}\right)} \tag{6}$$

$$\mathrm{DoU_{mixture}} = \frac{1}{2}\left(2 \times \mathrm{CN_{mixture}} + 2 - \mathrm{HN_{mixture}}\right) \tag{7}$$

Table 4. PC-SAFT parameter correlations as a function of MW (g/mol) for n-alkanes and PNAs using the GC parameters of [42]

	n-alkane	PNA
m	$0.0274\mathrm{MW} + 0.4648$	$0.0163\mathrm{MW} + 0.9256$
$m\sigma$ (Å)	$0.1092\mathrm{MW} + 1.5677$	$0.0612\mathrm{MW} + 3.5324$
$\varepsilon/_k$ (K)	$\exp(5.5811 - 10.2507/\mathrm{MW})$	$\exp(5.5657 - 8.6620/\mathrm{MW})$

2.c. Thermodynamic solver (PC-SAFT + VLE)

The thermodynamic solver is employed to compute temperature, pressure, sound speed and enthalpy once the conservative variables have been updated. The inputs are the density, internal energy and mass fraction of the components. Three pure component parameters per compound (number of segments per chain, energy parameter and segment diameter) are specified for initialisation. Only an overview of the method is included in this section.

Algorithm

The algorithm is summarized in Figure 3. The main steps are:

1) **Filter**. This step is employed to decrease the computational time by reducing VLE calculations. By checking the molar fractions of the components, it can be determined whether only one phase exists. Isobaric-adiabatic lines can be computed using the initial conditions of the case of interest (temperature in the chamber, temperature of the fuel and pressure in the combustion chamber) to determine the molar fractions at which VLE is not expected. For example, as we can see in Figure 4, by performing an injection of n-dodecane at 363K in a combustion chamber at 900K and 11MPa, the nitrogen mole fraction at which the fuel starts vaporizing is close to 0.15 and there is not liquid phase at nitrogen mole fractions higher than 0.95 . In this case, it would be safe to consider that any mixture with a nitrogen molar fraction lower than 0.05 (Limit A) and higher than 0.95 (Limit B) will not be in a VLE state. The reason of choosing a low Limit A is to consider the pressure variations along the simulation, which have an important effect on the stability of n-dodecane / N2 mixtures.

2) **Stable state (one phase).** When knowing that the mixture is stable the molecular density of the mixture can be computed and used as an input to the PC-SAFT model. A Newton method is employed to compute the temperature that is needed to calculate the value of all other thermodynamic variables. The temperature dependent function used in the iterative method is the internal energy. The derivative of the internal energy with respect to the temperature at constant molecular density can be directly obtained as these are the independent variables of the PC-SAFT model. See Appendices 2 and 3.

Thermodynamic solver

- Inputs
  - From conservative variables: ρ,e,Y_i
  - Temperature and pressure from the previous time step
  - Specific values of each component: σ,ε/K,k_{ij},m
- 1) Compute the mole fraction of each component (x)
- IF ((x_N <Limit A) .OR. (x_N >Limit B)) THEN
- CALL Algorithm 1 (Stable state)
- ELSE
- CALL Algorithm 2 (Unknown state)
- END IF

Figure 3. Schematic representation of the thermodynamic solver

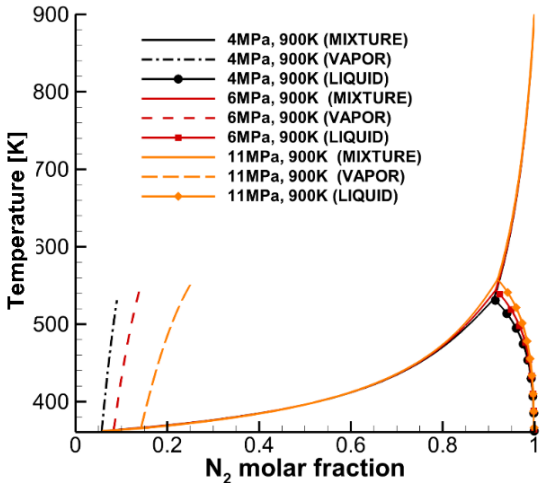

Figure 4. Isobaric-adiabatic mixing lines (N2 + C12H26) at different pressures in the combustion chamber

3) **Unknown state.** If the state of the mixture is unknown the density cannot be used as an input. The pressure and the temperature are iterated employing a multidimensional Newton method until the density and the internal energy obtained using the PC-SAFT + VLE calculations are the ones obtained from the conservative variables. For each P-T calculation a stability analysis is performed to determine if the mixture is stable. See Appendices 4 and 5.

   a. **Mixture stable:** The PC-SAFT model is solved. The reduced density is iterated until the computed pressure is the input pressure.

   b. **Mixture unstable:** The isothermal-isobaric flash problem (TPn flash) is solved and the properties of the fluid in a VLE state are computed.

Stability analysis

A mixture is stable at a specific T and P if the total Gibbs energy is at its global minimum. If an infinitesimal amount (δe) of a new phase of composition **w** is formed from a phase of composition **z,** the change in the Gibbs energy can be expressed as [44]:

$$\delta G = \delta e \sum_{i=1}^{C} w_i(\mu_i(\boldsymbol{w}) - \mu_i(\boldsymbol{z})) \quad (8)$$

μ being the chemical potential.

A necessary condition for the stability of the phase of composition **z** is that δG is non-negative for any positive δe for any composition **w.** This is known as the tangent plane condition of Gibbs.

$$\sum_{i=1}^{C} w_i(\mu_i(\boldsymbol{w}) - \mu_i(\boldsymbol{z})) \geq 0 \quad \forall \quad \mathrm{w}_i \geq 0 \quad \text{such that} \quad \sum_{i=1}^{C} w_i = 1 \tag{9}$$

The Tangent Plane Distance (TPD) function [45] is employed to determine if a split into two phases decreases the Gibbs energy.

$$TPD(\boldsymbol{w}) = \sum_{i=1}^{C} w_i(\mu_i(\boldsymbol{w}) - \mu_i(\boldsymbol{z})) \tag{10}$$

The TPD function can be written in a dimensionless form employing the fugacity coefficient (φ):

$$tpd(w_i) = \frac{TPD}{RT} = \sum_{i=1}^{C} w_i[ln\varphi_i(\boldsymbol{w}) + lnw_i - d_i(\boldsymbol{z})] \tag{11}$$

being

$$d_i(\boldsymbol{z}) = ln\varphi_i(\boldsymbol{z}) + lnz_i$$

The mixture of composition **z** is considered stable if all the TPD local minima are non-negative.

$$tpd(\boldsymbol{w}) \geq 0 \quad \forall \quad \mathrm{w}_i \geq 0 \quad \forall \quad \mathrm{w}_i \geq 0 \quad \text{such that} \quad \sum_{i=1}^{C} w_i = 1 \tag{12}$$

The Successive Substitution Iteration (SSI) algorithm ([16], [46]) (without the Newton method) has been employed to determine if the mixture is stable. See Appendix 6.

TPn flash

Once it is known that the mixture is in a VLE state, a multidimensional Newton iteration in T and P is performed until the internal energy and density of the liquid-gas mixture are the ones determined by the conservative variables. An isothermal-isobaric flash problem (known as TPn flash) is performed for each iteration.

A necessary condition for equilibrium is that the chemical potential for each component is the same in the liquid and vapor phases.

$$\mu_i^L = \mu_i^V \tag{13}$$

or equivalently using the fugacities:

$$f_i^L = f_i^V \tag{14}$$

Employing the fugacity coefficients, this expression can be written as:

$$F_i = ln\varphi_v(T,p,y) - ln\varphi_l(T,p,x) + lnK_i = 0 \tag{15}$$

where

$$K_i = \frac{x_i}{y_i} = \frac{\varphi_{i,l}}{\varphi_{i,v}} \tag{16}$$

A successive substitution method is employed to perform equilibrium calculations at specified temperature, pressure and overall composition to determine the liquid and vapor phases that satisfy eq.15 [16], [44]. See Appendix 7.

2.d. VLE interface

In [10], molecular dynamic simulations of three n-alkane fuels into nitrogen under various temperatures and pressures were performed to study the injection, evaporation and mixing processes of hydrocarbon fuels into a supercritical environment. The study was focused on understanding the transition from classical two-phase evaporation to one-phase diffusion-controlled mixing. Using as threshold a dimensionless transition time (the time needed to transit from subcritical to supercritical respect to the liquid lifetime) of 0.35, the authors identified two regions on the P-T diagram, see Figure 5. Supercritical dominated: Due to the high critical pressures of TYPE IV mixtures, a VLE state is present at the beginning of the evaporation process. The temperature of the liquid core goes up until the VLE state disappears and only a diffusion-controlled mixing process exists. Subcritical dominated: A clear interface exists between the liquid core and the ambient gases. Nitrogen is not able to diffuse into the liquid core (constant fuel mass fraction close to 1 during evaporation, see Figure 7). There is a gradual decrease of the density of the liquid core as the fuel is heated-up. The evaporation reaches a constant state with a constant liquid core.

According to the classification presented by [10], the combustion chamber of a Diesel engine working at medium-high load operation conditions is in the supercritical dominated regime after the compression cycle, see Figure 5. At these ambient conditions, the nitrogen is able to rapidly diffuse into the liquid core indicating that the interface has a Knudsen-number low enough to fall within the fluid mechanic continuum domain [7]. At 20MPa, the molar fraction of nitrogen in the liquid core (before the transition to a diffusion-controlled mixing process) at 0.5ns is almost 20%, see Figure 6. Therefore, the heat-up of the liquid core is dominated by diffusion phenomena. This can be proven by showing how isobaric-adiabatic mixing lines can replicate the heat-up profiles obtained in the molecular simulations of [10]. The isobaric-adiabatic lines where computed using eq.17. Figure 7 clearly shows how this hypothesis is not applicable in the subcritical dominated regime where after 5 ns the N_2 molar fraction in the liquid core has a constant value of 2%.

$$h_{mixture} = y_{C_{12}H_{26}} h_{C_{12}H_{26}} + y_{N_2} h_{N_2} \qquad (17)$$
$$p = 20MPa$$

being y the mass fraction.

The hypothesis employed in this paper is that the vaporization process at high-pressure Diesel fuel injections is located at the subcritical vaporization stage of the supercritical vaporization regime described by [10] without a transition to the diffusion-controlled mixing process. Being the convective forces much more dominant than the diffusion phenomena, N_2-n-dodecane mixing takes place in a time several orders of magnitude lower than the one observed in Figure 6 where only diffusion is present. Thus, the heat-up of the jet describes a single isobaric-adiabatic mixing line instead of multiple adiabatic lines at different times. This can be corroborated observing the results obtained by [15], [16] where the heat-up of the heat follows an isobaric-adiabatic mixing line constant in time solving both, convection and diffusion phenomena in their simulations. A diffuse interface method, which describe an adiabatic heat-up of the jet, must be applied during Diesel engine injection simulations at high-pressure conditions (supercritical dominated regime) to properly characterize how the fuel vaporize.

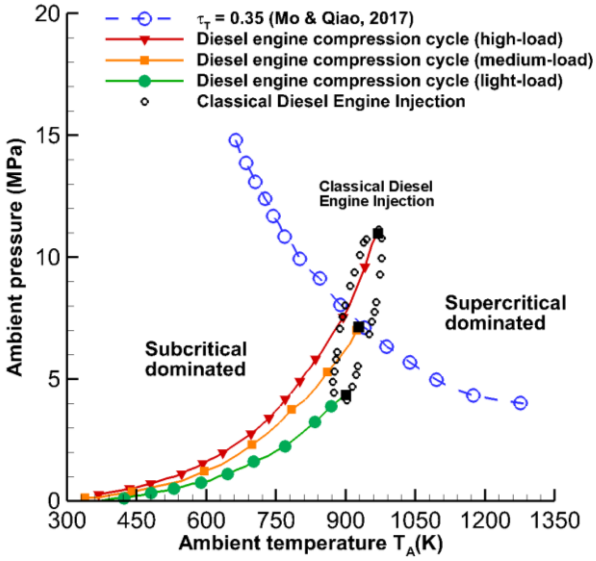

Figure 5. Diesel engine compression cycles [15] **and contours of dimensionless transition time on pressure-temperature diagram of n-dodecane** [10]

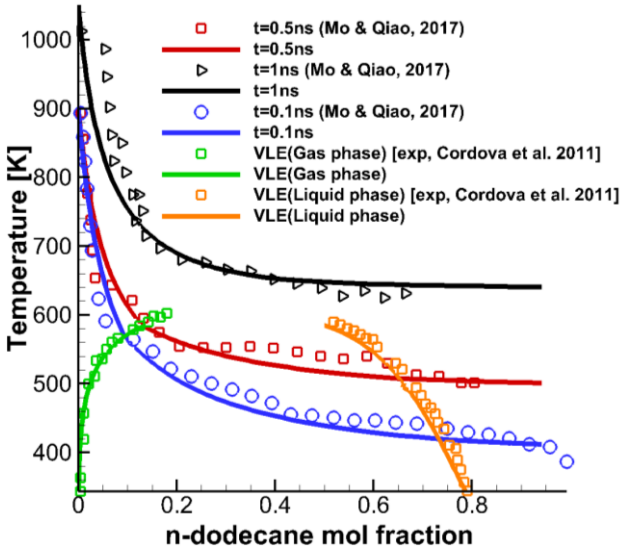

Figure 6. Development of gas–liquid interface shown on VLE diagram at 20 MPa [10]**, VLE experimental data** [38] **and isobaric-adiabatic mixing lines.**

3. Results

The working fluids employed are the following: (i) n-dodecane, (ii) a mixture of n-octane, n-dodecane and n-hexadecane; (iii) a pseudo-component that replicate the properties of the previous mixture; (iv) V0A Diesel, and (v) a pseudo-component that replicate the properties of the V0A Diesel.

3.a Shock Tube Problems

Shock Tube Problem 1 (One phase, one component)

A shock tube problem is used to validate the numerical solution of the hyperbolic operator. The results are compared with an exact solution computed using the methodology described in [47].

N-dodecane is utilized as working fluid; the domain is x ϵ [-0.5, 0.5] m; 300 equally spaced cells were employed; wave transmissive boundary conditions are used in the left and right sides; the simulated time is 5 10^{-4}s; the initial conditions in the left state are $\rho_L=438kg/m^3$, $p_L= 30MPa$, $u_L=0m/s$; and in the right state are $\rho_R=100kg/m^3$, $p_R=10MPa$, $u_R=0m/s$. Figure 8 shows how the density, temperature, velocity and pressure results agree with the exact solution.

Shock Tube Problem 2 (One phase, multicomponent/pseudo-component)

The working fluids employed are a mixture of n-octane, n-dodecane and n-hexadecane (Table 5) and a pseudo-component that replicate the properties of the mixture (Table 6) [41]. Figure 9 shows a comparison of the results obtained employing the multicomponent mixture and the results obtained by [41].

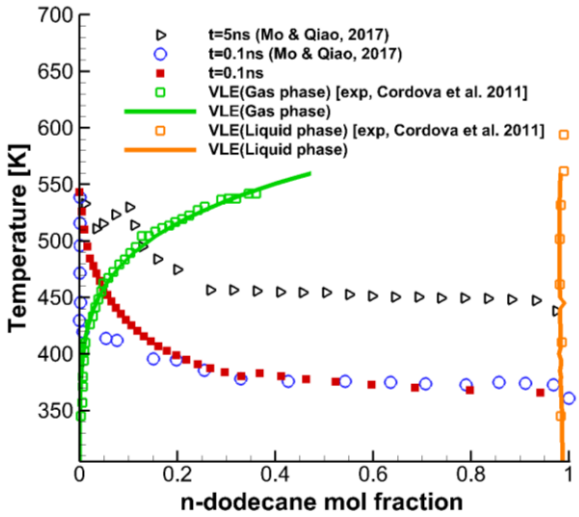

Figure 7. Development of gas–liquid interface shown on VLE diagram at 1 MPa [10]**, VLE experimental data** [38] **and isobaric-adiabatic mixing line.**

The domain is x ϵ [-0.5, 0.5] m; 800 equally spaced cells were employed; wave transmissive boundary conditions are used in the left and right sides; the simulated time is 5 10^{-4}s; the initial conditions in the left state are $\rho_L=438kg/m^3$, $t_L= 859.5K$, $u_L=0m/s$; and in the right state are $\rho_R=100kg/m^3$, $t_R=1744K$, $u_R=0m/s$. Figure 10 presents the density, temperature, pressure, velocity, speed of sound and internal energy results. The pseudo-component results are the same as the multicomponent ones indicating that the methodology developed by [41] can be used to model complex hydrocarbon mixtures as a pseudo-component in CFD simulations that present one phase.

Table 5. Molar composition of hydrocarbon mixture employed in Shock Tube Problem 2 [41]

Compound	Hydrocarbon mixture (Molar composition)
n-hexadecane	0.232
n-octane	0.460
n-dodecane	0.232

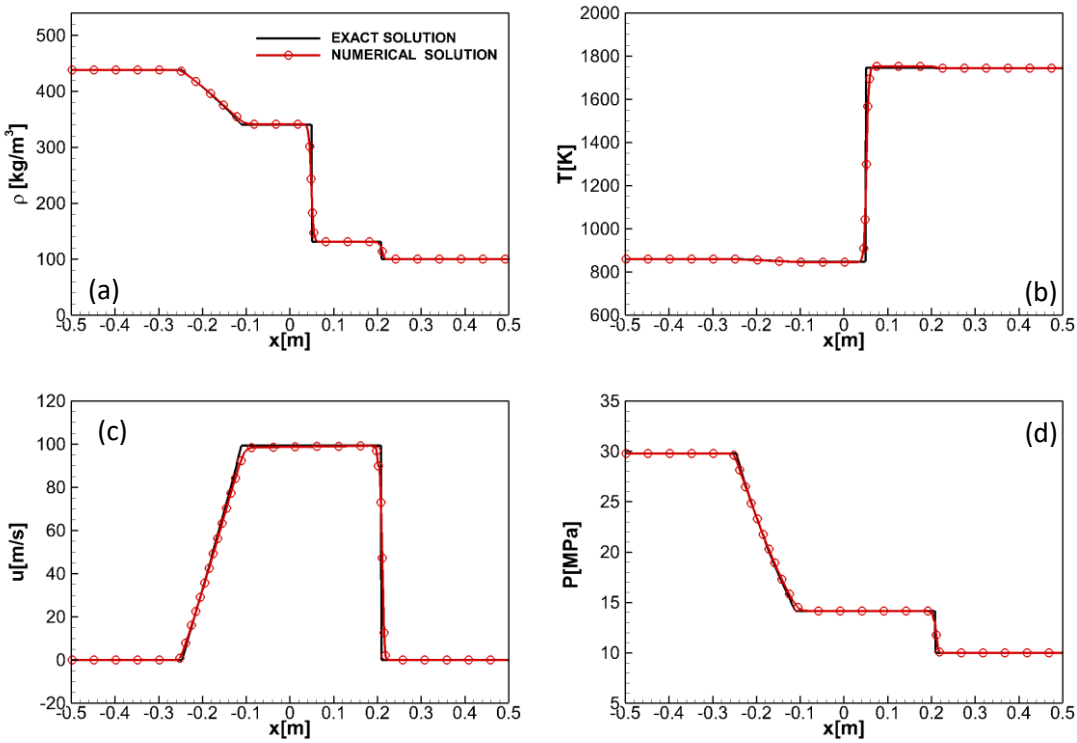

Figure 8. Shock Tube Problem ($C_{12}H_{26}$). CFL = 0.5, u = 0 m/s, 300 cells, t=5 10^{-4} s. Comparisons of (a) density, (b) temperature, (c) velocity and (d) pressure profiles: exact solution and numerical solutions.

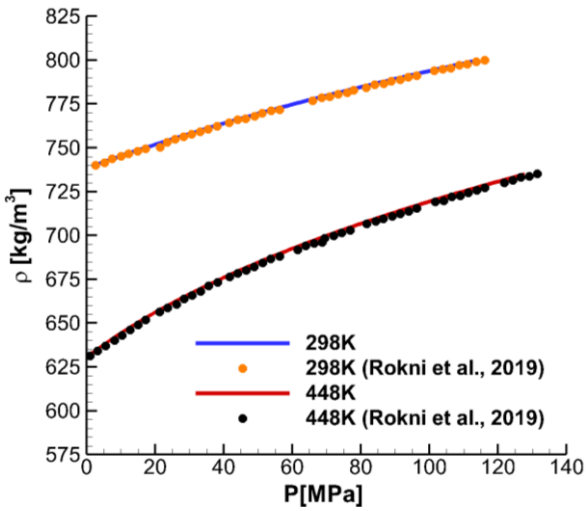

Figure 9. Density predictions for the hydrocarbon mixture presented in Table 5.

Table 6. PC-SAFT pure component parameters employed to model the pseudo-component employed in Shock Tube Problem 2 [41]

Compound	m	σ (Å)	ε/k (K)
Pseudo-component	7.387	3.400	234.47

3.b Advection test cases

The computational domain is x ϵ [-10^{-5}, 10^{-5}] m; the simulated time is 10^{-6}s; the left initial conditions are fuel at p=11MPa, u=10.0m/s and t=362K; the right initial conditions are nitrogen at p=11MPa, u=10.0m/s and t=972K; a uniform grid spacing (100 cells) is applied; CFL is set to be 0.5; wave transmissive boundary conditions are implemented in the left and right sides of the computational domain; and a smooth initial interface is applied to reduce the initial start-up error [48]. When a diffuse interface method is employed, the interfaces are not sharp one-point jumps but smooth as they are resolved [48]. Thus, a smooth initial profile is a realistic initial condition. The initial interface was computed employing eq.18 [16] **.**

$$Y_{FUEL} = 0.5 - 0.5erf\{(x_1 + 0.25l_{ref})/(0.01l_{ref})\} \tag{18}$$

The initialization of each cell located in the interface is performed knowing the pressure, enthalpy of the mixture (eq.17) and the molar fraction of the components.

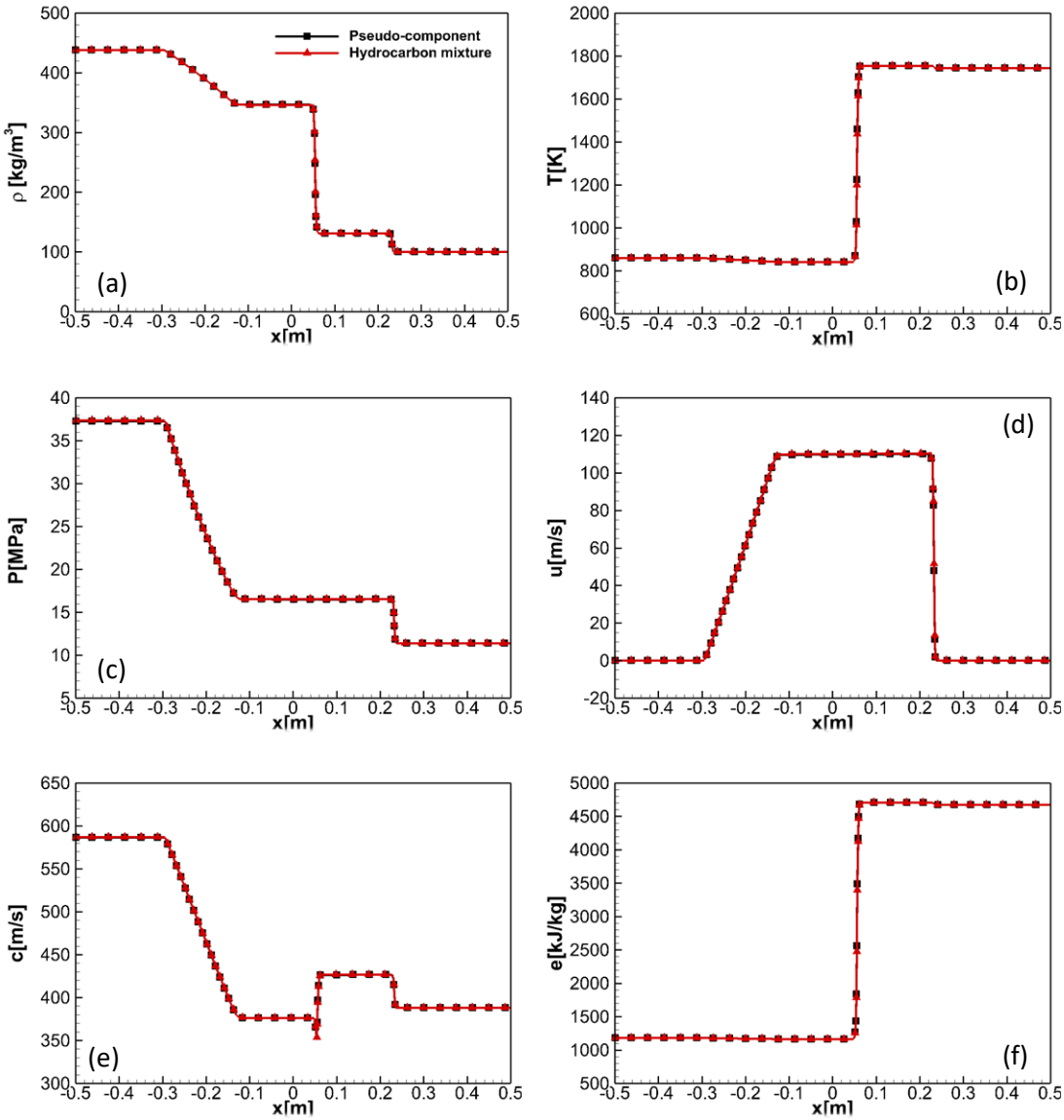

Figure 10. Shock Tube Problem 2. CFL = 0.5, 800 cells, t=5 10^{-4} s. Comparison of the (a) density, (b) temperature, (c) pressure, (d) x-velocity, (e) sonic fluid velocity, (f) internal energy using as working fluids are a mixture of n-octane, n-dodecane and n-hexadecane (Table 5) and a pseudo-component that replicate the properties of the mixture (Table 6) [41].

Advection test cases 1 (Two phases, n-dodecane/nitrogen)

Figure 11 shows the results of this advection test case where n-dodecane is employed as fuel. The binary interaction parameter applied is k_{ij} = 0.1446. The numerical framework perfectly captures the large density and temperature gradients present in this multicomponent-multiphase one-dimensional test case. Small spurious pressure oscillations appear in the solution. This problem is well known in multicomponent density based codes employing highly non-linear EoS [16], [19], [33]. Although the small oscillations in the pressure field could be avoided or reduced employing a QC formulation like the double flux model [32]–[34] or using a pressure evolution equation [16], [49], [50] instead of the total energy conservation equation , these schemes presents an error in the energy conservation that produce an unphysical quick heat-up of the fuel [16], [51]. The combination of VLE + PC-SAFT calculations allows to properly model: (1) the properties of n-dodecane at high density ranges where cubic models show large deviations in the sonic fluid velocity (used in density based CFD codes to compute the hyperbolic fluxes and time step [19]), temperature and internal energy; (2) and a correct (adiabatic) subcritical evaporation process in the interface (Section 2.d).

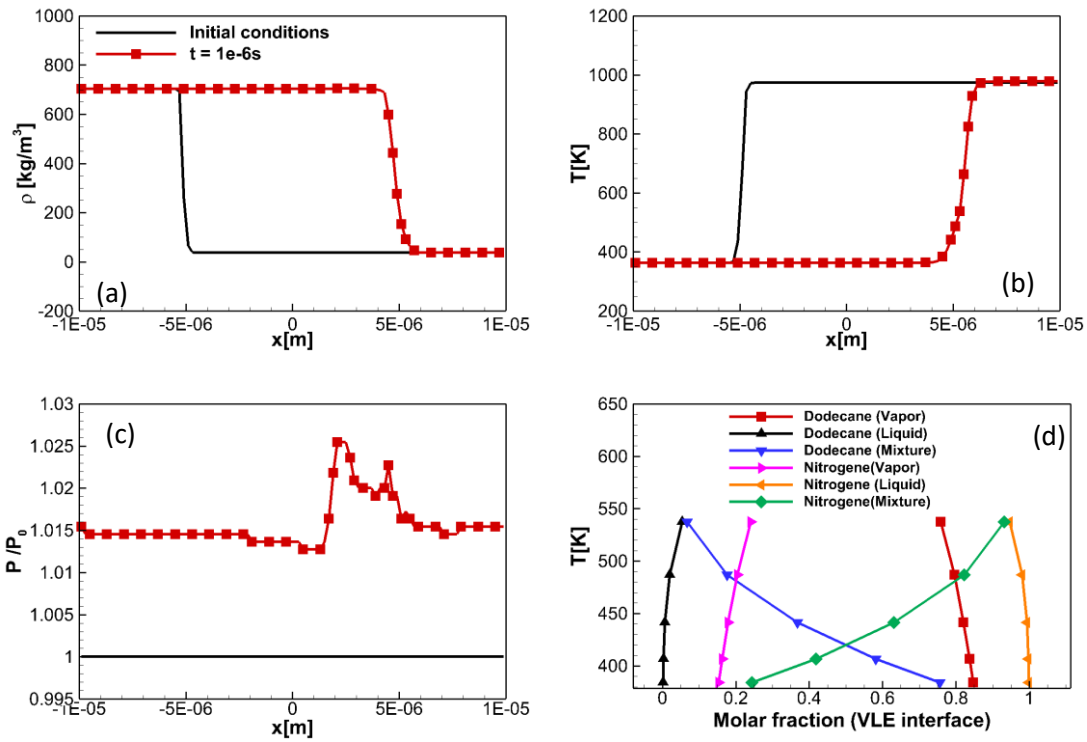

Figure 11. Advection Test Case 1 (N_2- $C_{12}H_{26}$), CFL = 0.5, u = 10 m/s, 100 cells. Results of (a) density, (b) temperature, (c) pressure and (d) VLE interface at 10^{-6}s.

Advection test case 2 (Two phases, V0A Diesel/ nitrogen, pseudo - V0A Diesel / nitrogen)

Figure 12 shows the temperature, density, speed of sound and internal energy results of an advection test case that employs the multicomponent Diesel V0A and the pseudo-Diesel V0A (Table 7) as fuels. The binary interaction parameter used between the nitrogen and the Diesel compounds or the pseudo-component is the same one used in the N_2 / n-dodecane mixture (kij = 0.1446). The pseudo-component presents an error (using as reference the multicomponent Diesel results) of 1.6% in density, 3.7% in sonic fluid velocity and 5.5% in internal energy. However, the computational time required to solve the multicomponent V0A Diesel advection test case is 432% the time consumed by the pseudo-Diesel advection test case. The different computational requirements will be even bigger in multidimensional cases or

simulations where the hydrocarbon mixture presents more components (e.g., V0B, V1 and V2 Diesel surrogates). In the case of the Diesel surrogate V0a, the equilibrium state of five components must be computed in each cell of the interface, see Figure 13. Using the methodology of [41], the number of working fluids is limited to 2 (pseudo-Diesel + N_2).

Figure 14 shows how the phase boundary from VLE at 11MPa is different if the multicomponent Diesel V0A or its pseudo-component are employed. The use of a pseudo-component must not alter how the fuel is heat-up, especially in Diesel injection simulations where the temperature plays a significant role on determining the ignition time. Figure 15 presents the results in the VLE interface of both working fluids (multicomponent mixture and pseudo-component).

Table 7. Pseudo-component PC-SAFT parameters employed to model the pseudo-Diesel V0A using the correlations developed by utilizing the GC parameters of Tihic et al. [42]

Compound	m	σ (Å)	$\varepsilon/_k$ (K)
Pseudo-component	5.436	3.908	256.700

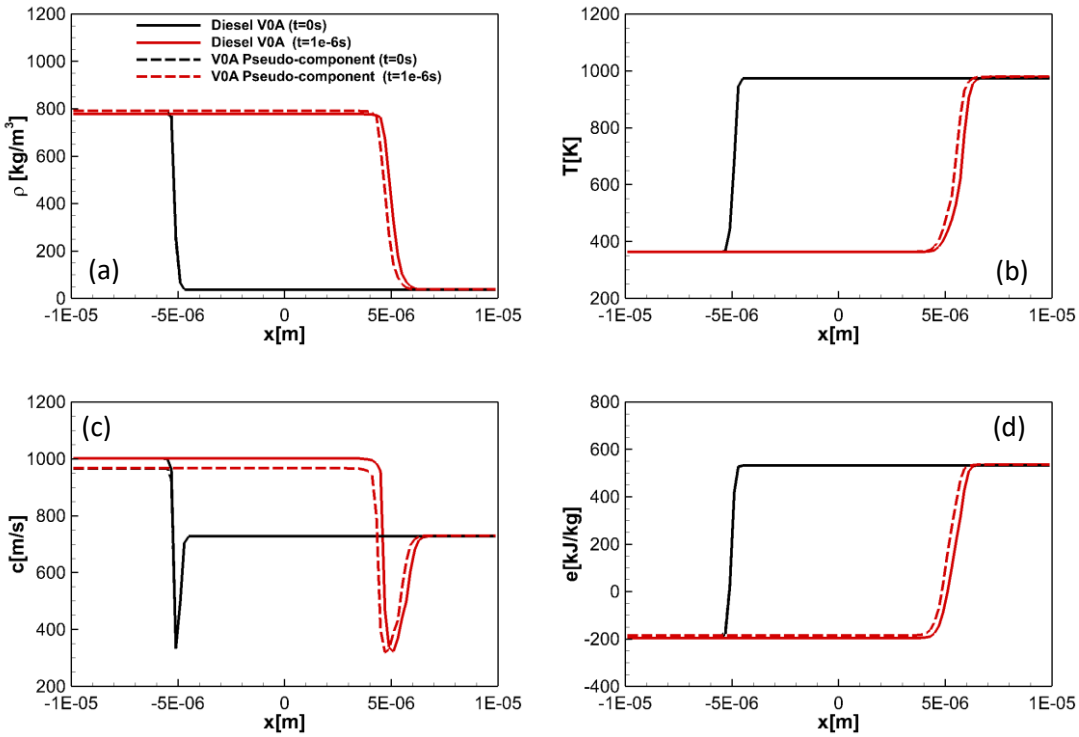

Figure 12. Advection Test Case 2 (N_2- V0A/ pseudo-Diesel V0A), CFL = 0.5, u = 10 m/s, 100 cells. Results of (a) density, (b) temperature, (c) speed of sound and (d) internal energy results at 10^{-6} s.

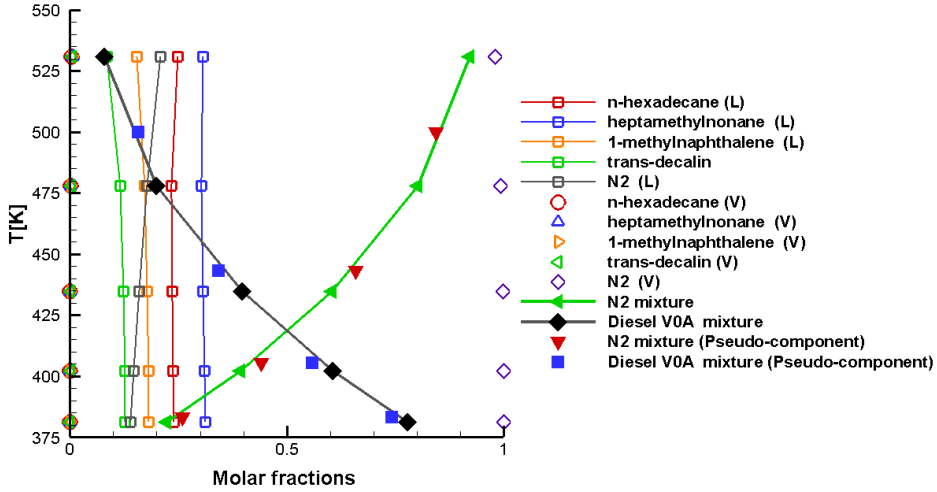

Figure 13. VLE Interface, Advection Test Case 2 (N_2- V0A/ pseudo-Diesel V0A), CFL= 0.5, u = 10 m/s, 100 cells. Results of VLE interface at 10^{-6}s.

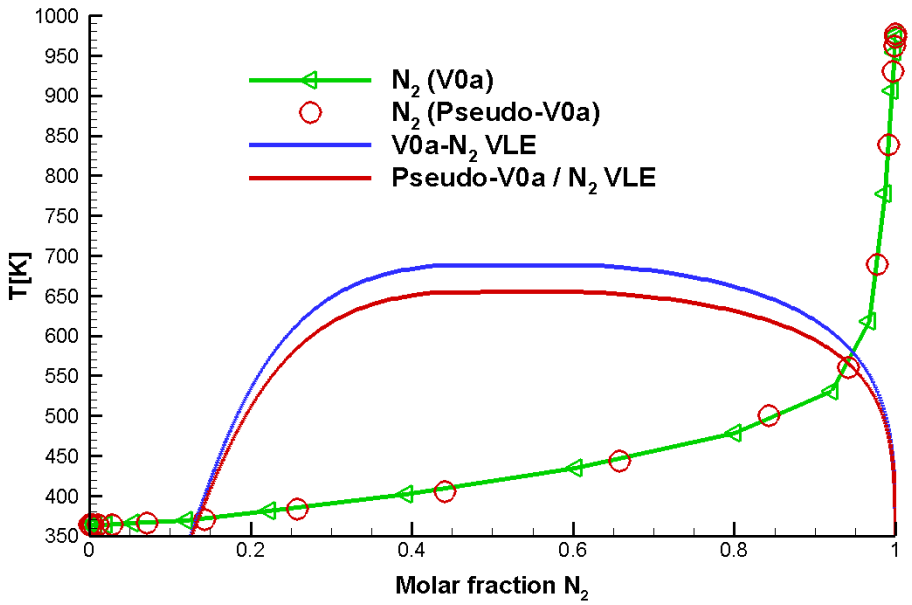

Figure 14. Advection Test Case 2 (N_2- V0A/ pseudo-Diesel V0A). Results of VLE interface at 10^{-6}s and phase boundaries from VLE at 11MPa.

3.c Two-dimensional cases

Planar two-dimensional injections of n-dodecane and a Diesel pseudo-component are presented to demonstrate the multidimensional capability of the numerical framework.

N-dodecane jet

A structured mesh is applied with a uniform cell distribution; the domain used is 12mm × 6mm; 1,216,800 cells are employed; the parabolic sub-step is included into these simulations without sub-grid scale modelling for turbulence or heat/species diffusion; the CFL number is set at 0.5; the fifth-order WENO discretization scheme presented in [18] is used; transmissive boundary conditions are applied at the top, bottom and right boundaries while a wall condition is employed at the left boundary; a flat velocity profile is imposed at the inlet; the velocity of

the jet is 600 m/s; the diameter of the exit nozzle is 0.1mm; the case is initialized using a pressure in the chamber of 11 MPa; the temperature of the nitrogen is 973 K; and the temperature of the injected fuel is 363K. The binary interaction parameter applied is k_{ij} = 0.1446. The loops where the hyperbolic fluxes, parabolic fluxes, update of conservative variables and thermodynamic solver are solved (see Figure 2) were paralleled employing OpenMP (24 physical cores where employed). Some instabilities were observed in the initialization as [16] reported. To solve this problem, a ramp is used to accelerate the fuel to 600m/s. The jet is quickly heated-up from a compressed liquid state to gas and finally, to a supercritical state describing an isobaric-adiabatic mixing line, see Figure 16. Figure 17 shows how the Kelvin Helmholtz instability and ligament-shaped structures are developed in the shear layer.

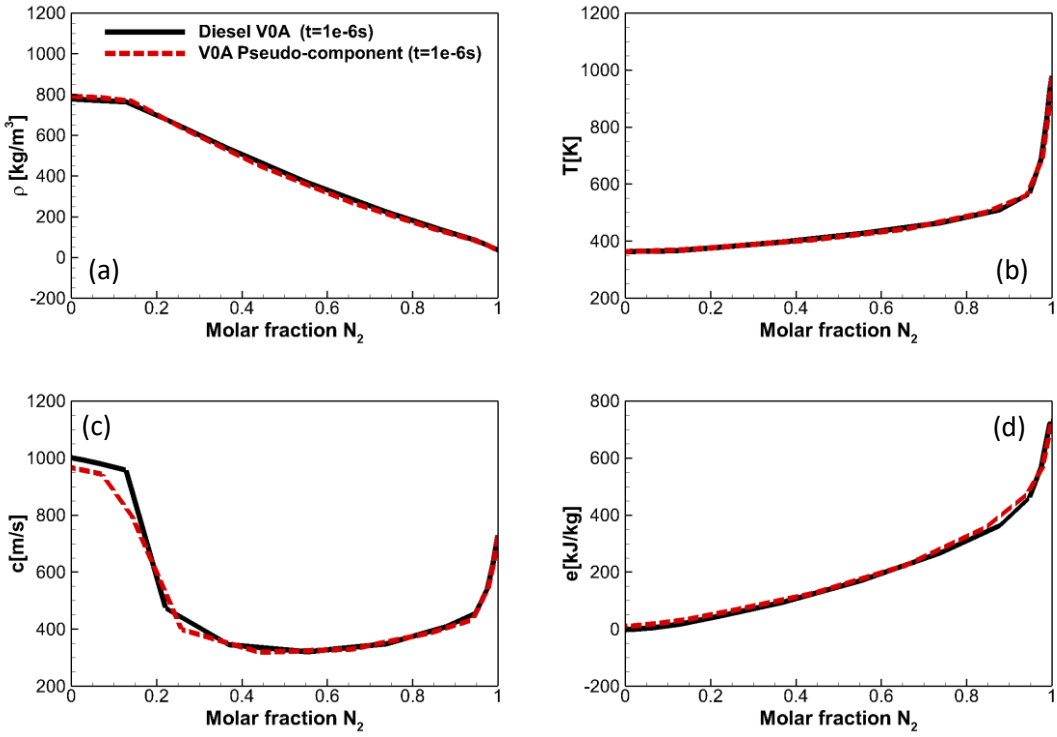

Figure 15. Advection Test Case 2 (N_2- V0A/ pseudo-Diesel V0A), CFL = 0.5, u = 10 m/s, 100 cells. Results of (a) density, (b) temperature, (c) speed of sound and (d) internal energy results at 10^{-6} s.

Diesel jet

The initial conditions and set-up of the simulation is the same as the n-dodecane jet. The binary interaction parameter applied is k_{ij} = 0.1446. Figure 18 shows the density, temperature and pressure at 3.19×10^{-5} s. Spurious pressure oscillations are not present in the pressure field despite the multicomponent nature of the simulations and large density gradients solved. The simulation present supersonic, transonic and subsonic regions due to the low values of the speed of sound present in the cells in a VLE state and the high jet velocity, see Figure 18. Such a variety of Mach numbers in a simulation can introduce important stability issues However, stability problems were not observed. The computational time required to solve at 3.3×10^{-5}s was 91.7 hours. Most time is invested on solving the multidimensional Newton method of the cells that are in a VLE state. At these conditions, the derivatives of the Jacobian matrix are calculated numerically (Appendix 5). However, the developed methodology is fast

enough to perform simulations at affordable time scales. It should also be considered that the results are equivalent to a multicomponent injection of a Diesel surrogate of 4 components that vaporize when mixed with hot nitrogen.

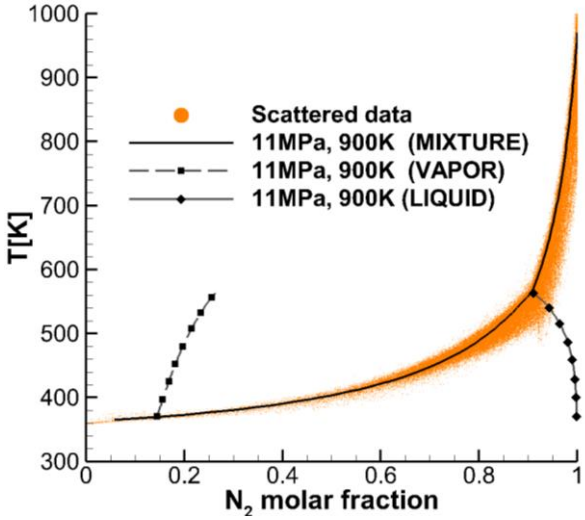

Figure 16. Scattered data of composition and temperature of the planar n-dodecane jet, dodecane-nitrogen phase boundary from VLE at 11MPa and isobaric-adiabatic mixing line.

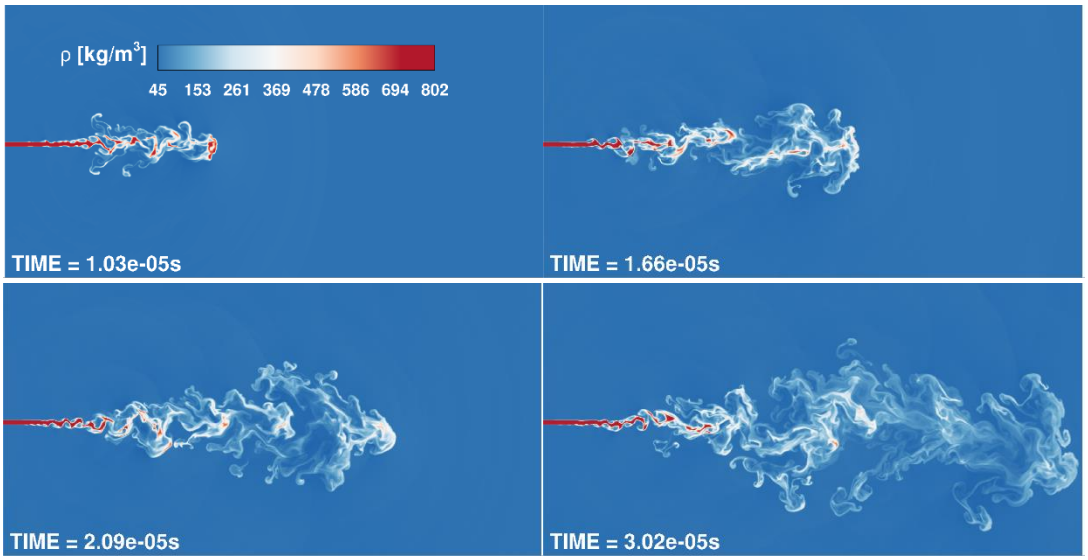

Figure 17. Density results of n-dodecane planar jet.

4. Conclusions

This paper presents a numerical framework that combines PC-SAFT and VLE calculations in a density-based, fully conservative solver of the Navier-Stokes and energy conservation equations to simulate fuel-air mixing at high-pressure conditions. This molecular-based EoS requires three empirically determined but well-known parameters to model the properties of a specific component, and thus, there is no need for extensive model calibration, as is typically the case when the NIST (REFPROP) library is utilised. PC-SAFT can flexibly handle the thermodynamic properties of multi-component mixtures for which the NIST (REFPROP) library supports only limited component combinations. Modelling multicomponent Diesel

surrogates, the PC-SAFT EoS shows the highest degree of agreement with experimental values in comparison with the results obtained using the model developed at NIST. Moreover, a purely predictive method that employs the PC-SAFT EoS for developing pseudo-components has been completed and validated to be used in CFD simulations. Complex hydrocarbon mixtures can be modelled as a single pseudo-component knowing its MW and HN/CN ratio. By employing pseudo-components, the simulation time is independent of the number of compounds present in the fuel and thus, allowing real fuel compositions to be utilised in CFD simulations. Advection test cases and shock tube problems were performed to validate the numerical framework using analytical and exact solutions. The two-dimensional simulations performed (subcritical injections of n-dodecane and Diesel into nitrogen) demonstrate the multidimensional, multispecies and multiphase capability of the algorithm and its high stability in simulations where all sonic regimes are present.

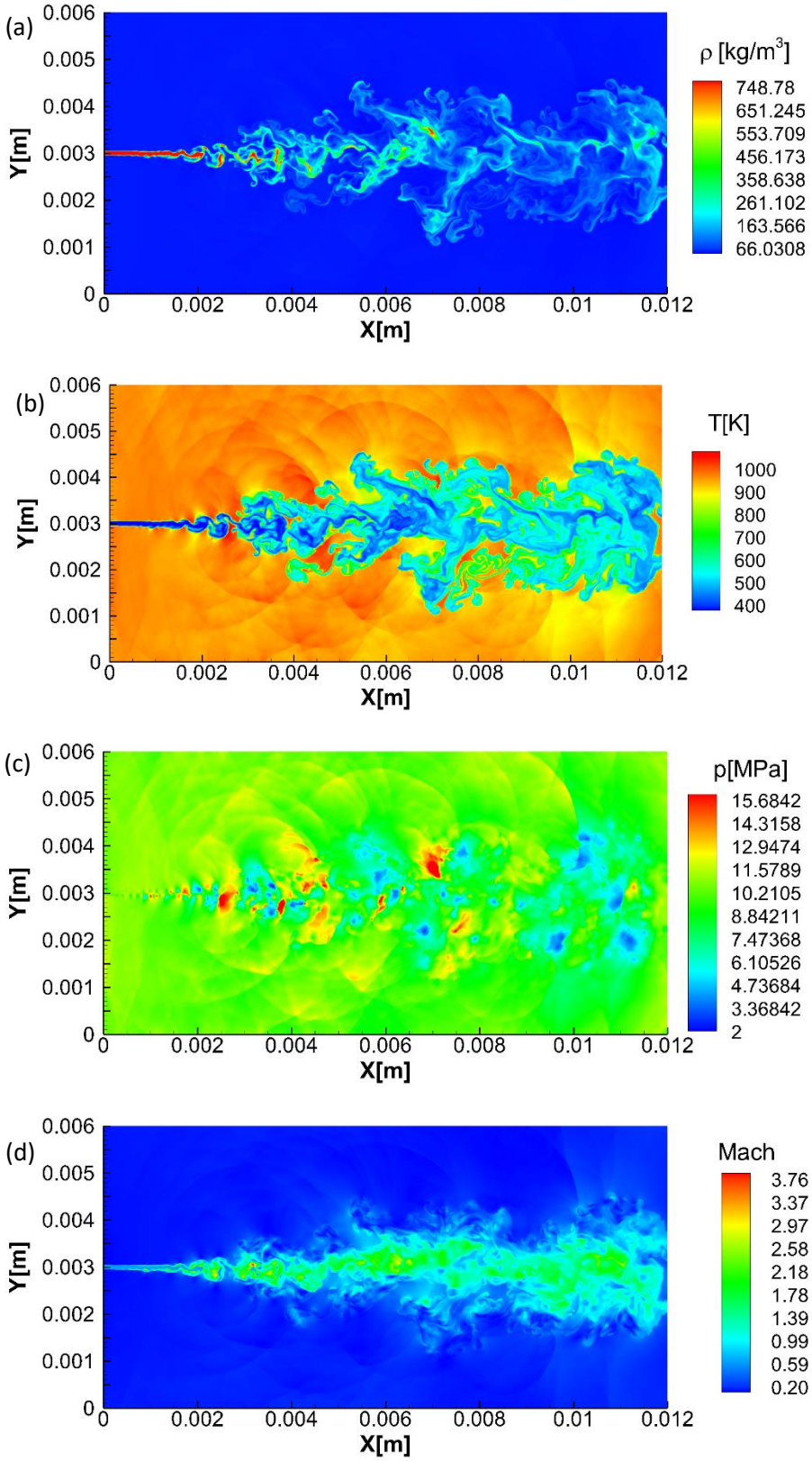

Figure 18. CFL = 0.5, 1,216,800 cells. Results of the simulation of the V0A Diesel pseudo-component jet at t = 3.19 x 10^{-5} s: (a) density, (b) temperature, (c) pressure and (d) Mach number.

Appendix 1 (CFD CODE)

The Navier-Stokes equations for a non-reacting multi-component mixture containing N species in a x-y 2D Cartesian system are given by:

$$\frac{\partial \boldsymbol{U}}{\partial t} + \frac{\partial \boldsymbol{F}}{\partial x} + \frac{\partial \boldsymbol{G}}{\partial y} = \frac{\partial \boldsymbol{F_v}}{\partial x} + \frac{\partial \boldsymbol{G_v}}{\partial y} \tag{A.1}$$

The vectors of A.1 are:

$$\mathbf{U} = \begin{bmatrix} \rho Y_1 \\ \vdots \\ \rho Y_N \\ \rho u \\ \rho v \\ \rho E \end{bmatrix}, \mathbf{F} = \begin{bmatrix} \rho u Y_1 \\ \vdots \\ \rho u Y_N \\ \rho u^2 + p \\ \rho u v \\ (\rho E + p)u \end{bmatrix}, \mathbf{G} = \begin{bmatrix} \rho v Y_1 \\ \vdots \\ \rho v Y_N \\ \rho v u \\ \rho v^2 + p \\ (\rho E + p)v \end{bmatrix}, \mathbf{F_v} = \begin{bmatrix} J_{x,1} \\ \vdots \\ J_{x,N} \\ \sigma_{xx} \\ \sigma_{xy} \\ u\sigma_{xx} + v\sigma_{xy} - q_x \end{bmatrix}, \tag{A.2}$$

$$\mathbf{G_v} = \begin{bmatrix} J_{y,1} \\ \vdots \\ J_{y,N} \\ \sigma_{yx} \\ \sigma_{yy} \\ u\sigma_{yx} + v\sigma_{yy} - q_y \end{bmatrix}$$

where ρ is the fluid density, u and v are the velocity components, p is the pressure, E is the total energy, J_i is the mass diffusion flux of species i, σ is the deviatoric stress tensor and q is the diffusion heat flux vector.

Hyperbolic sub-step

The multicomponent HLLC (Harten-Lax-van Leer-Contact) solver is applied to solve the Riemann problem [36]. The fluxes are computed as:

$$\mathbf{F}^{\mathrm{HLLC}} = \begin{cases} \mathbf{F}_L & \text{if} \quad 0 \le S_L, \\ \mathbf{F}_{*L} = \mathbf{F}_L + S_L(\mathbf{U}_{*L} - \mathbf{U}_L) & \text{if} \quad S_L \le 0 \le S_*, \\ \mathbf{F}_{*R} = \mathbf{F}_R + S_R(\mathbf{U}_{*R} - \mathbf{U}_R) & \text{if} \quad S_* \le 0 \le S_{*R}, \\ \mathbf{F}_R & \text{if} \quad 0 \ge S_{*R}, \end{cases} \tag{A.3}$$

where $\boldsymbol{U}_*$ are the star states [36].

The speed in the middle wave is:

$$S_* = \frac{p_R - p_L + \rho_L u_L (S_L - u_L) - \rho_R u_R (S_R - u_R)}{\rho_L (S_L - u_L) - \rho_R (S_R - u_R)} \tag{A.4}$$

The left and right wave speeds are computed as:

$$S_L = min(u_L - a_L, u_R - a_R),$$
$$S_R = max(u_L + a_L, u_R + a_R) \tag{A.5}$$

The conservative variables, pressure and speed of sound values needed to solve the Riemann problem are interpolated at the cell faces from cell centers using the fifth order reconstruction scheme described in [18]. This technique decreases the computational time and smooths-out the spurious pressure oscillations associated with fully conservative (FC) schemes employed along with real-fluid EoS.

The temporal integration is carried out using a second-order Runge–Kutta (RK2) scheme (A.6) applying the filter presented in [18].

$$\boldsymbol{U}^{(1)} = \boldsymbol{U}^{n} + \Delta t H_{xy}(\boldsymbol{U}^{n}),$$
$$\boldsymbol{U}^{n+1} = \frac{1}{2}\boldsymbol{U}^{n} + \frac{1}{2}\left[\boldsymbol{U}^{(1)} + \Delta t H_{xy}(\boldsymbol{U}^{(1)})\right] \tag{A.6}$$

Parabolic sub-step

The model developed by [37] is used to calculate the dynamic viscosity and the thermal conductivity. The viscous stress tensor is calculated as:

$$\sigma_{xx} = 2\mu_v \frac{\partial u}{\partial x} - \frac{2}{3}\mu_v \left(\frac{\partial u}{\partial x} + \frac{\partial v}{\partial y}\right)$$
$$\sigma_{yy} = 2\mu_v \frac{\partial v}{\partial y} - \frac{2}{3}\mu_v \left(\frac{\partial u}{\partial x} + \frac{\partial v}{\partial y}\right)$$
$$\sigma_{xy} = \sigma_{yx} = \mu_v \left(\frac{\partial u}{\partial y} + \frac{\partial v}{\partial x}\right) \tag{A.7}$$

where μ_v is the viscosity.

The species mass diffusion flux of species i is calculated employing Fick's law:

$$J_i = \rho D_i \nabla Y_i - Y_i \sum_{j=1}^{Nc} \rho D_j \nabla Y_j \tag{A.8}$$

where

$$D_i = \frac{(1-z_i)}{\sum_{j\neq i}^{Nc} \frac{z_j}{Di_j}} \tag{A.9}$$

being D is the diffusion coefficient for the diffusion of the component i in the rest of the mixture [52].

The heat flux vector is calculated as:

$$\boldsymbol{q} = -\lambda \nabla T - \sum_{i}^{N} h_i J_i \tag{A.10}$$

where λ is the thermal conductivity and h is the enthalpy.

Appendix 2 (Thermodynamic solver for stable mixtures)

The molecular density is computed using the density of the mixture. Once the molecular density is known a Newton method is employed to compute the temperature that is needed to calculate the value of all other thermodynamic variables. The temperature dependent function used in the iterative method is the internal energy. Initially a temperature value is assumed (for example the value of the temperature from the previous time RK sub-step or from the previous time step) to initialize the iteration process. In most cells, this value is close to the solution.

Algorithm 1

```
! Newton method (T)
DO
    1 CONTINUE
    If [(abs (e(CSV)-e(PC-SAFT))>0.001] then
        Algorithm A { Inputs: Temperature, density, molar composition
                      Outputs: Pressure, sonic fluid velocity, internal energy, enthalpy,
                               partial derivative of the internal energy respects
                               the temperature at constant density
        Compute the new temperature value:
        T^{n+1} = T^n + (∂e/∂T)_ρ T^n
        GO TO 1
    ELSE
        RETURN
    END IF
END DO
```

Figure A1. Schematic representation of the Algorithm 1

Appendix 3 (Algorithm A)

Inputs: Temperature, density, molar composition.

Output: Pressure, sonic fluid velocity, internal energy, enthalpy, partial derivative of the internal energy respects the temperature at constant density.

Algorithm A

1) Compute molecular density (A.11)
2) Compute segment diameter of each component (A.12)
3) Compute mean segment number (A.13)
4) Compute radial distribution function of the hard sphere fluid (A.14)
5) Compute hard sphere fluid contribution to the compressibility factor (A.16)
6) Compute hard chain contribution to the compressibility factor (A.17)
7) Compute dispersion contribution to the compressibility factor (A.19)
8) Compute total compressibility factor (A.30)
9) Compute pressure (A.31)
10) Compute the contribution of the hard-sphere system to the residual Helmholtz free energy temperature derivative (A.32)
11) Compute the hard-chain reference contribution to the residual Helmholtz free energy temperature derivative (A.35)
12) Compute the dispersion contribution to the residual Helmholtz free energy temperature derivative (A.37)
13) Compute the residual Helmholtz free energy temperature derivative (A.41)
14) Compute internal energy (A.43)
15) Compute enthalpy (A.45)
16) Compute heat capacities (A.46,A.47)
17) Compute sonic fluid velocity (A.50)
18) Compute the temperature derivative of the internal energy (A.58)
19) Compute the new temperature using the Newton-Raphson method

Figure A2. Schematic representation of the Algorithm A

Steps

1) **Compute molecular density**

$$\rho_m = \rho(kg/m^3)*10^{-30}*\mathrm{N}_A/\mathrm{M}_M*1000 \quad \text{(A.11)}$$

where N_A is the Avogadro number and M_M is the molecular weight of the mixture.

2) **Compute temperature-dependent segment diameter d of component i** [53]

$$d_i = \sigma_{di}\left[1 - 0.12\, exp\left(-3\,\frac{\varepsilon_i}{kT}\right)\right] \quad \text{(A.12)}$$

where k is the Boltzmann constant, T is the temperature, ε_i is the depth of pair potential of the component and σ_{di} is the segment diameter.

3) **Compute mean segment number** [53]

$$\bar{m} = \sum_i^{nc} x_i\, m_i \quad \text{(A.13)}$$

where m_i is the number of segments per chain of the component i and x_i is the mole fraction of component i.

4) **Compute radial distribution function of the hard-sphere fluid** [53]

$$g_{ij}^{hs} = \frac{1}{(1-\varsigma_3)} + \left(\frac{d_i d_j}{d_i+d_j}\right)\frac{3\varsigma_2}{(1-\varsigma_3)^2} + \left(\frac{d_i d_j}{d_i+d_j}\right)^2 \frac{3\varsigma_2^2}{(1-\varsigma_3)^3} \tag{A.14}$$

where

$$\varsigma_n = \frac{\pi}{6}\rho_m \sum_i x_i\, m_i d_i^n \qquad n \in \{0,1,2,3\} \tag{A.15}$$

5) **Compute contribution of the hard sphere to the compressibility factor** [53]

$$Z^{hs} = \frac{\varsigma_3}{(1-\varsigma_3)} + \frac{3\varsigma_1\varsigma_2}{\varsigma_0(1-\varsigma_3)^2} + \frac{3\varsigma_2^3 - \varsigma_3\varsigma_2^3}{\varsigma_0(1-\varsigma_3)^3} \tag{A.16}$$

6) **Compute hard-chain contribution to the compressibility factor** [53]

$$Z^{hc} = \bar{m}Z^{hs} - \sum_i x_i\,(m_i - 1)(g_{ii}^{hs})^{-1}\rho_m \frac{\partial g_{ii}^{hs}}{\partial \rho_m} \tag{A.17}$$

$$\rho\frac{\partial g_{ij}^{hs}}{\partial \rho} = \frac{\zeta_3}{(1-\zeta_3)^2} + \left(\frac{d_i d_j}{d_i+d_j}\right)\left(\frac{3\zeta_2}{(1-\zeta_3)^2} + \frac{6\zeta_2\zeta_3}{(1-\zeta_3)^3}\right) + \left(\frac{d_i d_j}{d_i+d_j}\right)^2\left(\frac{4{\zeta_2}^2}{(1-\zeta_3)^3} + \frac{6{\zeta_2}^2\zeta_3}{(1-\zeta_3)^4}\right) \tag{A.18}$$

7) **Compute dispersion contribution to the compressibility factor** [53]

$$Z^{disp} = -2\pi\rho_m \frac{\partial(\eta I_1)}{\partial \eta}\overline{m^2\varepsilon{\sigma_d}^3} - \pi\rho_m\bar{m}\left[C_1\frac{\partial(\eta I_2)}{\partial\eta} + C_2\eta I_2\right]\overline{m^2\varepsilon^2{\sigma_d}^3} \tag{A.19}$$

C_1 and C_2 are defined as:

$$C_1 = \left(1 + Z^{hc} + \rho\frac{\partial Z^{hc}}{\partial\rho}\right)^{-1} = \left(1 + \overline{m}\frac{8\eta - 8\eta^2}{(1-\eta)^4} + (1-\overline{m})\frac{20\eta - 27\eta^2 + 12\eta^3 - 2\eta^4}{[(1-\eta)(2-\eta)]^2}\right)^{-1} \tag{A.20}$$

$$C_2 = \frac{\partial C_1}{\partial\eta} = -C_1^2\left(\overline{m}\frac{-4\eta^2 + 20\eta + 8}{(1-\eta)^5} + (1-\overline{m})\frac{2\eta^3 + 12\eta^2 - 48\eta + 40}{[(1-\eta)(2-\eta)]^3}\right) \tag{A.21}$$

The terms $\overline{m^2\varepsilon{\sigma_d}^3}$ and $\overline{m^2\varepsilon^2{\sigma_d}^3}$ are defined as:

$$\overline{m^2\varepsilon{\sigma_d}^3} = \sum_i^{nc}\sum_j^{nc} x_i\, x_j m_i m_j \left(\frac{\varepsilon_{ij}}{kT}\right)\sigma_{d,ij}^3 \tag{A.22}$$

$$\overline{m^2\varepsilon^2{\sigma_d}^3} = \sum_i^{nc}\sum_j^{nc} x_i\, x_j m_i m_j \left(\frac{\varepsilon_{ij}}{kT}\right)^2\sigma_{d,ij}^3 \tag{A.23}$$

The mixture parameters σ_{ij} and ε_{ij} ,which are defined for every pair of unlike segments, are modelled using a Berthelot-Lorentz combining rule.

$$\sigma_{ij} = \frac{1}{2}(\sigma_i + \sigma_j) \tag{A.24}$$

$$\varepsilon_{ij} = \sqrt{\varepsilon_i\varepsilon_j}(1 - k_{ij}) \tag{A.25}$$

$\frac{\partial(\eta I_1)}{\partial\eta}$ and $\frac{\partial(\eta I_2)}{\partial\eta}$ are expressed as:

$$\frac{\partial(\eta I_1)}{\partial\eta} = \sum_{j=0}^{6} a_j\,(\bar{m})(j+1)\eta^i \tag{A.26}$$

$$\frac{\partial(\eta I_2)}{\partial\eta} = \sum_{j=0}^{6} b_j\,(\bar{m})(j+1)\eta^i \tag{A.27}$$

The coefficients a and b depend on the chain length:

$$a_i(\overline{m}) = a_{0i} + \frac{\overline{m}-1}{\overline{m}}a_{1i} + \frac{\overline{m}-1}{\overline{m}}\frac{\overline{m}-2}{\overline{m}}a_{2i} \tag{A.28}$$

$$b_i(\overline{m}) = b_{0i} + \frac{\overline{m}-1}{\overline{m}} b_{1i} + \frac{\overline{m}-1}{\overline{m}}\frac{\overline{m}-2}{\overline{m}} b_{2i} \tag{A.29}$$

$a_{0i}, a_{1i}, a_{2i}, b_{0i}, b_{1i}, b_{2i}$ are constants [53].

8) **Compute compressibility factor** [53]

$$Z = 1 + Z^{hc} + Z^{disp} \tag{A.30}$$

9) **Compute pressure** [53]

$$P = Zk_BT\rho_m(10^{10})^3 \tag{A.31}$$

10) **Compute temperature derivative of the Helmholtz free energy residual contribution of the hard-sphere system** [53]

$$\left(\frac{\partial \tilde{a}^{hs}}{\partial T}\right)_{\rho,x_i} = \frac{1}{\varsigma_0}\left[\begin{array}{c}\frac{3(\varsigma_{1,T}\varsigma_2+\varsigma_1\varsigma_{2,T})}{(1-\varsigma_3)} + \frac{3\varsigma_1\varsigma_2\varsigma_{3,T}}{(1-\varsigma_3)^2} + \frac{3{\varsigma_2}^2\varsigma_{2,T}}{\varsigma_3(1-\varsigma_3)^2} + \frac{{\varsigma_2}^3\varsigma_{3,T}(3\varsigma_3-1)}{{\varsigma_3}^2(1-\varsigma_3)^3} + \\ \left(\frac{3{\varsigma_2}^2\varsigma_{2,T}\varsigma_3-2{\varsigma_2}^3\varsigma_{3,T}}{{\varsigma_3}^3}\right) ln(1-\varsigma_3) + \left(\varsigma_0 - \frac{{\varsigma_2}^3}{{\varsigma_3}^2}\right)\frac{\varsigma_{3,T}}{(1-\varsigma_3)}\end{array}\right] \tag{A.32}$$

with abbreviations for two temperature derivatives:

$$\varsigma_{n,T} = \frac{\partial \varsigma_n}{\partial T} = \frac{\pi}{6}\rho\sum_i x_i\, m_i n d_{i,T}(d_i)^{n-1} \qquad n \in \{0,1,2,3\} \tag{A.33}$$

$$d_{i,T} = \frac{\partial d_i}{\partial T} = \sigma_i\left(3\frac{\varepsilon_i}{kT^2}\right)\left[-0.12\, exp\left(-3\frac{\varepsilon_i}{kT}\right)\right] \tag{A.34}$$

11) **Compute temperature derivative of the Helmholtz free energy hard-chain reference contribution** [53]

$$\left(\frac{\partial \tilde{a}^{hc}}{\partial T}\right)_{\rho,x_i} = \bar{m}\left(\frac{\partial \tilde{a}^{hs}}{\partial T}\right)_{\rho,x_i} - \sum_i x_i\,(m_i-1)({g_{ii}}^{hs})^{-1}\left(\frac{\partial {g_{ii}}^{hs}}{\partial T}\right)_{\rho,x_i} \tag{A.35}$$

The temperature derivative of the radial pair distribution function is:

$$\frac{\partial g_{ii}^{hs}}{\partial T} = \frac{\varsigma_{3,T}}{(1-\varsigma_3)^2} + \left(\frac{1}{2}d_{i,T}\right)\frac{\varsigma_2}{(1-\varsigma_3)^2} + \left(\frac{1}{2}d_i\right)\left(\frac{3\varsigma_{2,T}}{(1-\varsigma_3)^2} + \frac{6\varsigma_2\varsigma_{3,T}}{(1-\varsigma_3)^3}\right) + \left(\frac{1}{2}d_i d_{i,T}\right)\frac{2{\varsigma_2}^2}{(1-\varsigma_3)^3} + \left(\frac{1}{2}d_i\right)^2\left(\frac{4\varsigma_2\varsigma_{2,T}}{(1-\varsigma_3)^3} + \frac{6{\varsigma_2}^2\varsigma_{3,T}}{(1-\varsigma_3)^4}\right) \tag{A.36}$$

12) **Compute temperature derivative of the Helmholtz free energy dispersive attraction** [53]

$$\left(\frac{\partial \tilde{a}^{disp}}{\partial T}\right)_{\rho,x_i} = -2\pi\rho\left(\frac{\partial I_1}{\partial T} - \frac{I_1}{\partial T}\right)\overline{m^2\varepsilon{\sigma_d}^3} - \pi\rho\overline{m}\left[\frac{\partial C_1}{\partial T}I_2 + C_1\frac{\partial I_2}{\partial T} - 2C_1\frac{I_2}{T}\right]\overline{m^2\varepsilon^2{\sigma_d}^3} \tag{A.37}$$

with

$$\frac{\partial I_1}{\partial T} = \sum_{i=0}^{6} a_i(\overline{m})i\varsigma_{3,T}\eta^{i-1} \tag{A.38}$$

$$\frac{\partial I_2}{\partial T} = \sum_{i=0}^{6} b_i(\overline{m})i\varsigma_{3,T}\eta^{i-1} \tag{A.39}$$

$$\frac{\partial C_1}{\partial T} = \varsigma_{3,T} C_2 \tag{A.40}$$

13) Compute temperature derivative of the Helmholtz free energy [53]

$$\left(\frac{\partial \tilde{a}^{res}}{\partial T}\right)_{\rho,x_i} = \left(\frac{\partial \tilde{a}^{hc}}{\partial T}\right)_{\rho,x_i} + \left(\frac{\partial \tilde{a}^{disp}}{\partial T}\right)_{\rho,x_i} \tag{A.41}$$

14) Compute the internal energy [54]

The internal energy is estimated as the sum of the ideal internal energy and the residual internal energy [54].

$$\frac{e^{res}}{RT} = -T\left(\frac{\partial \tilde{a}^{res}}{\partial T}\right)_{\rho,x_i} \tag{A.42}$$

$$e = e^{res} + e^{id} \tag{A.43}$$

15) Compute enthalpy [53]**:**

It is computed as the sum of the ideal contribution (obtained by integrating the ideal heat capacity at constant pressure with respect to the temperature) and the residual enthalpy [53].

$$\frac{h^{res}}{RT} = -T\left(\frac{\partial \tilde{a}^{res}}{\partial T}\right)_{\rho,x_i} + (Z-1) \tag{A.44}$$

$$h = h^{res} + h^{id} \tag{A.45}$$

16) Heat capacities [55]

Heat capacities are computed as the sum of the ideal contribution [56] and the correction terms calculated with the PC-SAFT EoS [54]. where C_p and C_v are the heat capacities at constant pressure and volume respectively.

$$C_v = C_{v,id} + C_{v,res} \tag{A.46}$$

$$C_p = C_{p,id} + C_{p,res} \tag{A.47}$$

$$C_v^{res} = -RT\left[2\left(\frac{\partial \tilde{a}^{res}}{\partial T}\right)_{\rho,x_i} + T\left(\frac{\partial^2 \tilde{a}^{res}}{\partial T^2}\right)_{\rho,x_i}\right] \tag{A.48}$$

$$C_p^{res} = C_v^{res} + R\frac{\left[\rho_m T\left(\frac{\partial^2 \tilde{a}^{res}}{\partial \rho_m \partial T}\right)_{x_i} + \rho_m\left(\frac{\partial \tilde{a}^{res}}{\partial \rho_m}\right)_{T,x_i} + 1\right]^2}{\left[\rho_m{}^2\left(\frac{\partial^2 \tilde{a}^{res}}{\partial \rho_m{}^2}\right)_{T,x_i} + 2\rho_m\left(\frac{\partial \tilde{a}^{res}}{\partial \rho_m}\right)_{T,x_i} + 1\right]} \tag{A.49}$$

17) Speed of sound [55]

The speed of sound is computed as:

$$c = \sqrt{\frac{C_p}{C_v}\left(\frac{\partial P}{\partial \rho_m}\right)_T} \tag{A.50}$$

The derivatives needed to compute the speed of sound are:

$$\left(\frac{\partial P}{\partial \rho_m}\right)_{T,x_i} = \left(\frac{\partial P}{\partial \eta}\right)_{T,x_i}\left(\frac{\partial \eta}{\partial \rho_m}\right)_{T,x_i} \tag{A.51}$$

$$\left(\frac{\partial \eta}{\partial \rho_m}\right)_{T,x_i} = \frac{\pi}{6}\left(\sum_i x_i m_i d_i^3\right) \tag{A.52}$$

$$\left(\frac{\partial P}{\partial \eta}\right)_{T,x_i} = k_B T (10^{10})^3 \left[\rho_m \left(\frac{\partial Z}{\partial \eta}\right)_{T,x_i} + Z \left(\frac{\partial \rho_m}{\partial \eta}\right)_{T,x_i}\right] \tag{A.53}$$

$$\left(\frac{\partial \rho_m}{\partial \eta}\right)_{T,x_i} = \frac{6}{\pi}\left(\sum_i x_i m_i d_i^3\right)^{-1} \tag{A.54}$$

$\left(\frac{\partial Z}{\partial \eta}\right)_{T,x_i}$ can be found in [57]. (A.55)

18) Compute derivative internal energy respect temperature at constant density [55]

$$\left(\frac{\partial e^{res}}{\partial T}\right)_{\rho,x_i} = -RT\left[2\left(\frac{\partial \tilde{a}^{res}}{\partial T}\right)_{\rho,x_i} + \left(\frac{\partial^2 \tilde{a}^{res}}{\partial T^2}\right)_{\rho,x_i} * T\right] \tag{A.56}$$

$$\frac{de^{id}}{dT} = C_v^{id} \tag{A.57}$$

$$\left(\frac{\partial e}{\partial T}\right)_{\rho,x_i} = \left(\frac{\partial e^{res}}{\partial T}\right)_{\rho,x_i} + \frac{de^{id}}{dT} \tag{A.58}$$

19) Compute the new temperature using the Newton method

Appendix 4 (Thermodynamic solver for mixtures at an unknown state)

The pressure and the temperature are iterated employing a multidimensional Newton method until the density and the internal energy obtained in the PC-SAFT are the ones obtained from the conservative variables. The initial values of the pressure and the temperature are the ones already stored in the cell that is being solved.

Algorithm 2

```
!Multidimensional Newton (P,T)
DO
    2 CONTINUE
    If [(abs (e(CSV)-e(VLE))>0.001].AND.[(abs (ρ(CSV)-ρ(VLE))>0.001] then
        Perform Stabiblity Analisys (SSI)
        IF(STABLE = .TRUE.)
            Algorithm B { Inputs: Temperature, pressure, molar composition
                          Outputs: Density, sonic fluid velocity, internal energy, enthalpy,
                                   partial derivative of the internal energy respects
                                   the temperature at constant density
                                   (∂ρ/∂p)_t, (∂ρ/∂t)_p, (∂e/∂p)_t, (∂e/∂t)_p
        ELSE
            Call TPn algorithm
        END IF
    Compute the new temperature and pressure values:
```

$$\begin{bmatrix} p \\ t \end{bmatrix}_{n+1} = \begin{bmatrix} p \\ t \end{bmatrix}_{n} - \left[\mathbf{J}^{-1}(p,t)_n\right] \begin{bmatrix} \rho(p,t)_n \\ e(p,t)_n \end{bmatrix}$$

$$\mathbf{J} = \begin{bmatrix} \left(\frac{\partial \rho}{\partial p}\right)_t & \left(\frac{\partial \rho}{\partial t}\right)_p \\ \left(\frac{\partial e}{\partial p}\right)_t & \left(\frac{\partial e}{\partial t}\right)_p \end{bmatrix}$$

```
    GO TO 2
    ELSE
    RETURN
    END IF
END DO
```

Figure A3. Schematic representation of the Algorithm 2

Appendix 5 (Algorithm B)

Inputs: Temperature, pressure, molar composition.

Output: Density, speed of sound, internal energy, enthalpy, fugacities, partial derivative of the internal energy respect the temperature at constant pressure, partial derivative of the internal energy respect the pressure at constant temperature, partial derivative of the density respects the temperature at constant pressure and partial derivative of the density respect the temperature at constant pressure.

This algorithm is applied when the pressure and the temperature are iterated employing a multidimensional Newton method until the density and the internal energy computed are the ones obtained from the conservative variables.

$$\begin{bmatrix} p \\ t \end{bmatrix}_{n+1} = \begin{bmatrix} p \\ t \end{bmatrix}_{n} - \left[\boldsymbol{J}^{-1}(p,t)_n\right] \begin{bmatrix} \rho(p,t)_n \\ e(p,t)_n \end{bmatrix} \tag{A.59}$$

where

$$\boldsymbol{J} = \begin{bmatrix} \left(\frac{\partial \rho}{\partial p}\right)_t & \left(\frac{\partial \rho}{\partial t}\right)_p \\ \left(\frac{\partial e}{\partial p}\right)_t & \left(\frac{\partial e}{\partial t}\right)_p \end{bmatrix} \tag{A.60}$$

The independent variables of the PC-SAFT are the temperature and the density. Thus, it is necessary to perform the following transformations to obtain the partial derivatives needed for the multidimensional Newton method.

$$\left(\frac{\partial \rho}{\partial p}\right)_T = \left(\frac{\partial p}{\partial \rho}\right)_T^{-1} \qquad \text{Reciprocity} \tag{A.61}$$

$$\left(\frac{\partial \rho}{\partial t}\right)_p = -\left(\frac{\partial p}{\partial t}\right)_\rho \left(\frac{\partial p}{\partial \rho}\right)_T^{-1} \qquad \text{Chain rule} \tag{A.62}$$

$$\left(\frac{\partial e}{\partial p}\right)_T = \left(\frac{\partial e}{\partial \rho}\right)_T \left(\frac{\partial p}{\partial \rho}\right)_T^{-1} \qquad \text{Chain rule} \tag{A.63}$$

$$\left(\frac{\partial e}{\partial t}\right)_p = \left(\frac{\partial e}{\partial t}\right)_\rho - \left(\frac{\partial e}{\partial \rho}\right)_T \left(\frac{\partial \rho}{\partial t}\right)_\rho \left(\frac{\partial p}{\partial \rho}\right)_T^{-1} \qquad \text{Triple product rule} \tag{A.64}$$

The partial derivatives needed then are:

$$\left(\frac{\partial p}{\partial t}\right)_\rho, \left(\frac{\partial p}{\partial \rho}\right)_T, \left(\frac{\partial e}{\partial \rho}\right)_T, \left(\frac{\partial e}{\partial t}\right)_\rho$$

Steps

1) **Compute temperature-dependent segment diameter d of component i (A.12)**
2) **Compute mean segment number (A.13)**
3) **Compute radial distribution function of the hard-sphere fluid (A.14)**
4) **Reduce density iterative method**
    a. $\boldsymbol{\eta_{INIT}} = \mathbf{0.45}$
    b. **Compute contribution of the hard sphere to the compressibility factor (A.16)**
    c. **Compute hard-chain contribution to the compressibility factor (A.17)**

Algorithm B

1) Compute segment diameter of each component (A.12)
2) Compute mean segment number (A.13)
3) Compute radial distribution function of the hard sphere fluid (A.14)
4) Reduce density iterative method

$\eta_{INIT} = 0.45$
DO
If $\left[\left(\text{abs}\,(p^{calc} - p^{sys}\right) > 0.001\right]$ *then*
Compute hard sphere fluid contribution to the compressibility factor (A.16)
Compute hard chain contribution to the compressibility factor (A.17)
Compute dispersion contribution to the compressibility factor (A.19)
Compute total compressibility factor (A.30)
Compute pressure (A.31)
Derivative of pressure respect resuce density
Compute new pressure using Newton method
END IF
END DO

5) Compute the contribution of the hasd-sphere system to the residual Helmholtz free energy temperature derivative (A.32)
6) Compute the hard-chain reference contribution to the residual Helmholtz free energy temperature derivative (A.35)
7) Compute the dispersion contribution to the residual Helmholtz free energy temperature derivative (A.37)
8) Compute the residual Helmholtz free energy temperature derivative (A.41)
9) Compute internal energy (A.43)
10) Compute enthalpy (A.45)
11) Compute heat capacities (A.46,A.47)
12) Compute speed of sound (A.50)
13) Compute the derivatives of the Helmholtz free energy residual contribution of the hard-sphere system respect the molar fraction of the components (A.66)
14) Compute the derivative of the hard-chain reference contribution to the residual Helmholtz free energy respect the molar fraction of the components (A.68)

Algorithm B

15) Compute derivative of the dispersion contribution to the residual Helmholtz free energy respect the molar fraction of the components (A.70)
16) Compute the chemical potential (A.78)
17) Compute the fugacity coefficient (A.79)
18) Compute the partial derivative of the pressure respect the density at constant temperature (A.80)
19) Compute the partial derivative of the pressure respect the temperature at constant density (A.81)
20) Compute the partial derivative of the internal energy respect the temperature at contant density (A.58)
21) Compute the partial derivative of the internal energy respect the density at constant temperature (A.84)
22) Compute the partial derivative of the density respect the pressure at constant temperature (A.61)
23) Compute the partial derivative of the density respect the temperature at constant pressure (A.62)
24) Compute the partial derivative of the internal energy respect the pressure at constant temperature (A.63)
25) Compute the partial derivative of the internal energy respect the temperature at constant pressure (A.64)

Figure A4 Schematic representation of the Algorithm B

d. **Compute dispersion contribution to the compressibility factor (A.19)**
e. **Compute compressibility factor (A.30)**
f. **Compute pressure (A.31)**
g. **Derivative of pressure respect reduce density**

$$\left(\frac{\partial P}{\partial \eta}\right) = \left[\rho_m \left(\frac{\partial Z}{\partial \eta}\right) + Z\left(\frac{\partial \rho_m}{\partial \eta}\right)\right](10^{10})^3 Z k_B T \tag{A.65}$$

h. **Compute the new pressure using the Newton method**

5) **Compute temperature derivative of the Helmholtz free energy residual contribution of the hard-sphere system (A.32)**
6) **Compute temperature derivative of the hard-chain reference contribution to the residual Helmholtz free energy (A.35)**
7) **Compute temperature derivative of the dispersion contribution to the residual Helmholtz free energy (A.37)**
8) **Compute temperature derivative of the Helmholtz free energy (A.41)**
9) **Compute the internal energy (A.43)**
10) **Compute enthalpy (A.45)**
11) **Compute heat capacities (A.46-47)**
12) **Compute speed of sound (A.50)**
13) **Compute the derivatives of the Helmholtz free energy residual contribution of the hard-sphere system respect the molar fraction of the components.**

$$\left(\frac{\partial \tilde{a}^{hs}}{\partial x_k}\right)_{T,\rho,x_{j\neq k}} = -\frac{\zeta_{0,xk}}{\zeta_0}\tilde{a}^{hs} + \frac{1}{\zeta_0}\left[\frac{3(\zeta_{1,xk}\zeta_2+\zeta_1\zeta_{2,xk})}{(1-\zeta_3)} + \frac{3\zeta_1\zeta_2\zeta_{3,xk}}{(1-\zeta_3)^2} + \frac{3\zeta_2^2\zeta_{2,xk}}{\zeta_3(1-\zeta_3)^2} + \frac{\zeta_2^3\zeta_{3,xk}(3\zeta_3-1)}{{\zeta_3}^2(1-\zeta_3)^3} + \left(\frac{3\zeta_2^2\zeta_{2,xk}\zeta_3-2\zeta_2^3\zeta_{3,xk}}{{\zeta_3}^3} - \zeta_{0,xk}\right) ln(1-\zeta_3) + \left(\zeta_0 - \frac{\zeta_2^3}{\zeta_3^2}\right)\frac{\zeta_{3,xk}}{(1-\zeta_3)}\right] \tag{A.66}$$

where

$$\zeta_{n,xk} = \left(\frac{\partial \zeta_n}{\partial x_k}\right)_{T,\rho,x_{j\neq k}} = \frac{\pi}{6}\rho m_k (d_k)^n \tag{A.67}$$

14) **Compute the derivative of the hard-chain reference contribution to the residual Helmholtz free energy respect the molar fraction of the components.**

$$\left(\frac{\partial \tilde{a}^{hc}}{\partial x_k}\right)_{T,\rho,x_{j\neq k}} = m_k \tilde{a}^{hs} + \bar{m}\left(\frac{\partial \tilde{a}^{hs}}{\partial x_k}\right)_{T,\rho,x_{j\neq k}} - \sum_i x_i (m_i - 1)(g_{ii}^{hs})^{-1}\left(\frac{\partial g_{ii}^{hs}}{\partial x_k}\right)_{T,\rho,x_{j\neq k}} \tag{A.68}$$

where

$$\left(\frac{\partial g_{ij}^{hs}}{\partial x_k}\right)_{T,\rho,x_{j\neq k}} = \frac{\zeta_{3,xk}}{(1-\zeta_3)^2} + \left(\frac{d_i d_j}{d_i + d_j}\right)\left(\frac{3\zeta_{2,xk}}{(1-\zeta_3)^2} + \frac{6\zeta_2\zeta_{3,xk}}{(1-\zeta_3)^3}\right) + \left(\frac{d_i d_j}{d_i + d_j}\right)^2\left(\frac{4\zeta_2\zeta_{2,xk}}{(1-\zeta_3)^3} + \frac{6\zeta_2^2\zeta_{3,xk}}{(1-\zeta_3)^4}\right) \tag{A. 69}$$

15) Compute derivative of the dispersion contribution to the residual Helmholtz free energy respect the molar fraction of the components.

$$\left(\frac{\partial \tilde{a}^{disp}}{\partial x_k}\right)_{T,\rho,x_{j\neq k}} = -2\pi\rho\left[I_{1,xk}\overline{m^2\varepsilon\sigma^3} + I_1\overline{(m^2\varepsilon\sigma^3)}_{xk}\right] - \pi\rho\left\{\left[m_k C_1 I_2 + \overline{m}C_{1,xk}I_2 + \overline{m}C_1 I_{2,xk}\right]\overline{m^2\varepsilon\sigma^3} + \overline{m}C_1 I_2\overline{(m^2\varepsilon\sigma^3)}_{xk}\right\} \quad (A.70)$$

where

$$\overline{(m^2\varepsilon\sigma^3)}_{xk} = 2m_k\sum_j x_j m_j\left(\frac{\varepsilon_{kj}}{kT}\right)\sigma_{kj}^3 \quad (A.71)$$

$$\overline{(m^2\varepsilon^2\sigma^3)}_{xk} = 2m_k\sum_j x_j m_j\left(\frac{\varepsilon_{kj}}{kT}\right)^2\sigma_{kj}^3 \quad (A.72)$$

$$C_{1,xk} = C_2\zeta_{3,xk} - C_1^2\left[m_k\frac{8\eta-2\eta^2}{(1-\eta)^4} - m_k\frac{20\eta-27\eta^2+12\eta^3-2\eta^4}{[(1-\eta)(2-\eta)]^2}\right] \quad (A.73)$$

$$I_{1,xk} = \sum_{i=0}^{6}\left[a_i(\bar{m})i\zeta_{3,xk}\,\eta^{i-1} + a_{i,xk}\eta^i\right] \quad (A.74)$$

$$I_{2,xk} = \sum_{i=0}^{6}\left[b_i(\bar{m})i\zeta_{3,xk}\,\eta^{i-1} + b_{i,xk}\eta^i\right] \quad (A.75)$$

$$a_{i,xk} = \frac{m_k}{\overline{m}^2}a_{1i} + \frac{m_k}{\overline{m}^2}\left(3-\frac{4}{\overline{m}}\right)a_{2i} \quad (A.76)$$

$$b_{i,xk} = \frac{m_k}{\overline{m}^2}b_{1i} + \frac{m_k}{\overline{m}^2}\left(3-\frac{4}{\overline{m}}\right)b_{2i} \quad (A.77)$$

16) Compute the chemical potential.

$$\frac{\mu_k^{res}(T,v)}{kT} = \tilde{a}^{res} + (Z-1) + \left(\frac{\partial\tilde{a}^{res}}{\partial x_k}\right)_{T,v,x_{i\neq j}} - \sum_{j=1}^{N}\left[x_j\left(\frac{\partial\tilde{a}^{res}}{\partial x_j}\right)_{T,v,x_{i\neq j}}\right] \quad (A.78)$$

17) Compute the fugacity coefficient.

$$ln\varphi_k = \frac{\mu_k^{res}(T,v)}{kT} - ln\,Z \quad (A.79)$$

18) Compute the partial derivative of the pressure respect the density at constant temperature.

$$\left(\frac{\partial P}{\partial\rho_m}\right)_T = k_B T(10^{10})^3\left[\left(\frac{\partial Z}{\partial\rho_m}\right)_t\rho_m + Z\right] \quad (A.80)$$

19) Compute the partial derivative of the pressure respect the temperature at constant density.

$$\left(\frac{\partial P}{\partial T}\right)_\rho = k_B(10^{10})^3\rho_m\left[\left(\frac{\partial Z}{\partial T}\right)_\rho T + Z\right] \quad (A.81)$$

20) Compute the partial derivative of the inernal energy respect the temperature at constant density (A.58)

21) Compute the partial derivative of the internal energy respect the density at constant temperature.

$$\left(\frac{\partial e^{res}}{\partial\rho_m}\right)_T = -RT^2\left(\frac{\partial\tilde{a}^{res}}{\partial T\partial\rho_m}\right)_T \quad (A.82)$$

$$\frac{de^{id}}{d\rho_m} = 0.0 \tag{A.83}$$

$$\left(\frac{\partial e}{\partial T}\right)_{\rho,x_i} = \left(\frac{\partial e^{res}}{\partial T}\right)_{\rho,x_i} \tag{A.84}$$

22) Compute the partial derivative of the density respect the pressure at constant tmeperature (A.61)

23) Compute the partial derivative of the density respect the temperature at constant pressure (A.62)

24) Compute the partial derivative of the internal energy respect the pressure at constant temperature (A.63)

25) Compute the partial derivative of the internal energy respect the temperature at constant pressure (A.64)

Appendix 6 (Stability)

Input: Temperature, pressure and molar composition of the mixture.

Output: To know if the mixture is stable or not (one or two phases).

The Successive Substitution Iteration (SSI) algorithm ([16], [46]) (without the Newton method) has been employed.

```
Stability
1) IF (T > T_c FUEL) THEN
        STABLE=1
        RETURN
   END IF
2) IF[ (X_N2 > C).AND.(X_N2 < D)] THEN
        STABLE=0
        RETURN
   END IF
3) Call Algorithm B (obtain fugacity values)
      Inputs: Temperature, pressure, molar composition of the mixture
4) Calculate d_i(z) (A.75)
5) Wilcom´s correlation is used to initialize the K-values (A.76)
6) Calculaten Y_init (A.77-A.78 )
7) DO k=1,ntrial      ! SSI ALGORITHM
        Y_i = Y_init(k,i)
        DO j=1,nmax
           IF (‖dY‖>ε_SSI) THEN
                y_trial_i = Y_i /sum(Y)
                Call Algorithm B
                   Inputs: Temperature, pressure, molar composition y_trial
                   Obtain fugacity values (ln φ_i)
                Yn(i) = exp[d_i(z) − ln φ_i]
                dY_i = Yn_i - Y_i
                Y_i = Yn_i
           ELSE
                TPD*(k) = 1. - sum(Y)
                GO TO 1
           END IF
        END DO
 1 CONTINUE
IF (min(TPD*(k))< -10^-8
     STABLE = FALSE
ELSE
    STABLE =TRUE
END IF
END DO
```

Figure A5 Schematic representation of the stability algorithm

Steps

1) **The mixture is stable if the temperature is higher than T_c Fuel (STABLE = 1)**
   Any mixture with a temperature higher than the fuel critical temperature will not be in a VLE state (STABLE = 1). This kind of filters are applied to reduce the computational time.

2) **The mixture is unstable if the nitrogen molar fraction is bigger than C and lower than D (STABLE = 0)**
   The coefficients B and C are case dependent. For example, by performing an injection of n-dodecane at 363K in a combustion chamber at 900K, the nitrogen mole fraction at which the fuel starts vaporizing depends on the pressure in the combustion chamber. Considering Diesel engines at high-load operation conditions (11MPa) it would be safe to consider that any mixture with a nitrogen molar fraction bigger than 0.35 and lower than 0.7 will be in a VLE state, see Figure 4.

3) **Call Algorithm B to obtain fugacity coefficient values $\boldsymbol{ln\varphi_i(z_i)}$**
   Inputs: Temperature, pressure, molar composition of the mixture

4) **Calculate $d_i(z)$**
   $$d_i(z) = ln\varphi_i(z_i) + lnz_i \tag{A.85}$$

5) **The Wilcom´s correlation is used to initialize the K-values**
   $$K_i = \frac{p_{ci}}{p} exp\left[5.37(1.0 + w_i)\left(1.0 - \frac{T_{ci}}{T}\right)\right] \tag{A.86}$$
   being
   $$K_i = \frac{x_i}{y_i}$$
   where p_{ci} is the critical pressure of the component i, T_{ci} is the critical temperature of the component i, w_i is the acentric factor of the component i.

6) **Calculate trial phases Y (two trials)**

   For the trial 1:
   $$Y(1, comp) = \begin{cases} \frac{z_i}{K_i} \text{ (Liquid phase)} \\ z_i K_I \text{ (Vapor phase)} \end{cases} \tag{A.87}$$

   For the trial 2:
   $$Y(2, comp) = \begin{cases} \frac{z_i}{K_i 3} \quad \text{(Liquid phase)} \\ \frac{z_i K_I}{3} \quad \text{(Vapor phase)} \end{cases} \tag{A.88}$$

7) **SSI-Algorithm described in Figure A5**.

Appendix 7 (TPn Algorithm)

Input: Temperature, pressure and molar composition of the mixture.

Output: Density of the mixture, internal energy of the mixture, speed of sound of the mixture and enthalpy of the mixture.

This algorithm is employed to to perform equilibrium calculations at specified temperature, pressure and overall composition. A successive substitution method is employed [16], [44].

TPN

1) Wilcom´s correlation is used to initialize the K-values (A.86)
2) WHILE (eps(TPN)<10^{-7}) THEN
    !Rachford-Rice
    a) If the conditions A.89-A.90 are met:
        $\beta_{min}=0$, $\beta_{max}=1$
        If $K_i>1$ change β_{min} and β_{max} (A.91-A.92)
        Calculate β_{ini} (A.93)
        Change β_{min} and β_{max} (A.94)
        WHILE (eps(Rachford-Rice) > 10^{-7}) THEN
            Calculate g(β), $g'(\beta)$ (A.95-A.96)
            Change limits β_{min} and β_{max} (A.97)
            Newton-Raphson (A.98)
            Calculate $eps = abs\left(\left(\beta_{new}-\beta\right)/\beta\right)$
            New overall fraction of vapor phase (A.100-A.101)
        Calculate liquid and vapour mole fractions (A.102-A.103)
    b) If the conditions A.89-A.90 are not met:
        Calculate liquid and vapour mole fractions (A.104-A.105)
    c) Call Algorithm B to obtain fugacity coefficients of the liquid and vapor phase
    d) Objective function (A.106)
    e) Calculate eps(TPN)
    f) Update K-factors from fugacity coeffcients (A.107)
END
3) Calculate VLE properties

Figure A6 Schematic representation of the TPn algorithm

1) **The Wilcom´s correlation is used to initialize the K-values (A.86)**

2) **WHILE (eps(TPN)<10^{-7}) THEN**

Solve Rachford-Rice

a. **Check conditions A.79-A.80 to know if there is a solution in the interval** $\beta[0,1]$. **If the conditions are met set** $\beta_{\min}=0$, $\beta_{\max}=1$. **If not, go to step 2.b.**

$$\sum_{i=1}^{C} z_i K_i - 1 > 0 \qquad \text{(A.89)}$$

$$1 - \sum_{i=1}^{C} \frac{z_i}{K_i} < 0 \qquad \text{(A.90)}$$

- **If $K_i > 1$then**

$$\boldsymbol{\beta}_{\min} = max_i\left[0, \frac{K_i z_i - 1}{K_i - 1}\right] \quad (A.91)$$

$$\beta_{max} = min_i\left[1, \frac{1 - z_i}{1 - K_i}\right] \quad (A.92)$$

- **Calculate** $\beta_{ini} = 0.5(\beta_{min} + \beta_{max})$ (A.93)

- **Change limits**

$$g(\beta_{ini}) > 0 \rightarrow \beta_{min} = \beta_{ini},$$
$$g(\beta_{ini}) < 0 \rightarrow \beta_{max} = \beta_{ini} \quad (A.94)$$

- **WHILE (eps(Rachford-Rice) > 10^{-7}) then**

  - **Calculate** $g(\beta)$, $\boldsymbol{g'(\beta)}$

$$g(\beta) = \sum_{i=1}^{C}(y_i - x_i) = \sum_{i=1}^{C}\frac{z_i(K_i - 1)}{1 - \beta + \beta K_i} = 0 \quad (A.95)$$

$$g'(\beta) = -\sum_{i=1}^{C}\frac{z_i(K_i - 1)^2}{(1 - \beta + \beta K_i)^2} < 0 \quad (A.96)$$

  - **Change limits**

$$g > 0 \rightarrow \beta_{min} = \beta,$$
$$g < 0 \rightarrow \beta_{max} = \beta \quad (A.97)$$

  - **Newton-Raphson**

$$\Delta\beta = -\frac{g(\beta)}{dg/d\beta}$$
$$\beta_{new} = \beta + \Delta\beta \quad (A.98)$$

  - **Calculate eps**

$$eps = abs\big((\beta_{new} - \beta)/\beta\big) \quad (A.99)$$

  - **New overall fraction of vapor phase:**

$$\beta = \beta_{new} \text{ if } \beta_{new} \text{ is inside the interval } [\beta_{min}, \beta_{max}] \quad (A.100)$$

  - **If it is not, it is calculated as:**

$$\beta = 0.5(\beta_{min} + \beta_{max}), \quad \beta_{min} < \beta_{new} < \beta_{max} \quad (A.101)$$

  - **Calculate liquid and vapour mole fractions**

$$x_i = \frac{z_i}{1 - \beta + \beta K_i} \quad (A.102)$$

$$y_i = \frac{K_i z_i}{1 - \beta + \beta K_i} \quad (A.103)$$

b. If the conditions A.89-A.90 are not met [58]**:**

If $\sum z_i / K_i \leq 1$ the liquid and vapour mole fractions are computed as:

$$\beta = 1$$
$$x_i = z_i / K_i$$
$$y_i = z_i \quad (A.104)$$

Normalization of x_i

If $\sum z_i K_i \leq 1$ the liquid and vapour mole fractions are computed as:

$\beta = 0$

$x_i = z_i$

$y_i = z_i * K_i$ (A.105)

Normalization of y_i

c. **Call Algorithm B to obtain fugacity coefficients of the liquid and vapor phase**

Inputs: Temperature, pressure, molar composition of the liquid or vapor

d. **Objective function**

$F_i = ln\varphi_v(T,p,y) - ln\varphi_l(T,p,x) + lnK_i = 0$ (A.106)

e. **Calculate eps(TPN)**

f. **Update K-factors from fugacity coeffcients**

$K_i = exp(\, ln\varphi_l(T,p,x) - ln\varphi_v(T,p,y))$ (A.107)

3) Compute VLE properties

a. **The phase fraction on mass (β_m) basis is computed as:**

$$\beta_m = \beta \frac{M_V(\text{mixture molar mass in liquid phase})}{M_T(\text{mixture molar mass})} \quad \text{(A.108)}$$

b. **The equilibrium volume (v_{EQ}) is computed as:**

$v_{EQ} = \beta_m v_v + (1 - \beta_m) v_l$ (A.109)

c. **The equilibrium density is computed as:**

$\rho = \frac{1}{v_{EQ}}$ (A.110)

d. **The equilibrium internal energy is computed as:**

$e = \beta_m e_v + (1 - \beta_m) e_l$ (A.111)

e. **The equilibrium enthalpy is computed as:**

$h = \beta_m h_v + (1 - \beta_m) h_l$ (A.112)

f. **The speed of sound in the VLE state was computed using Wallis formula:**

$\frac{1}{\rho c_{wallis}^2} = \frac{\theta}{\rho_v c_v^2} + \frac{1-\theta}{\rho_l c_l^2}$ (A.113)

where the vapour volume fraction (θ) is computed as:

$\theta = \frac{\rho - \rho_v}{\rho_v - \rho_l}$ (A.114)

References

[1] W. O. H. Mayer *et al.*, "Atomization and Breakup of Cryogenic Propellants Under High-Pressure Subcritical and Supercritical Conditions," *J. Propuls. Power*, vol. 14, no. 5, pp. 835–842, Sep. 1998.

[2] C. Segal and S. A. Polikhov, "Subcritical to supercritical mixing," *Phys. Fluids*, 2008.

[3] R. R. Rachedi, L. C. Crook, and P. E. Sojka, "An Experimental Study of Swirling Supercritical Hydrocarbon Fuel Jets," *J. Eng. Gas Turbines Power*, 2010.

[4] B. Chehroudi, "Recent experimental efforts on high-pressure supercritical injection for liquid rockets and their implications," *International Journal of Aerospace Engineering*. 2012.

[5] M. Oschwald *et al.*, "Injection of fluids into supercritical environments," *Combust. Sci. Technol.*, 2006.

[6] R. N. Dahms, J. Manin, L. M. Pickett, and J. C. Oefelein, "Understanding high-pressure gas-liquid interface phenomena in Diesel engines," *Proc. Combust. Inst.*, 2013.

[7] R. N. Dahms and J. C. Oefelein, "On the transition between two-phase and single-phase interface dynamics in multicomponent fluids at supercritical pressures," *Phys. Fluids*, vol. 25, no. 9, 2013.

[8] J. Manin, M. Bardi, L. M. Pickett, R. N. Dahms, and J. C. Oefelein, "Microscopic investigation of the atomization and mixing processes of diesel sprays injected into high pressure and temperature environments," *Fuel*, vol. 134, pp. 531–543, 2014.

[9] C. Crua, J. Manin, and L. M. Pickett, "On the transcritical mixing of fuels at diesel engine conditions," *Fuel*, vol. 208, pp. 535–548, 2017.

[10] G. Mo and L. Qiao, "A molecular dynamics investigation of n-alkanes vaporizing into nitrogen: transition from subcritical to supercritical," *Combust. Flame*, vol. 176, pp. 60–71, 2017.

[11] Y. Pei, E. R. Hawkes, S. Kook, G. M. Goldin, and T. Lu, "Modelling n -dodecane spray and combustion with the transported probability density function method," *Combust. Flame*, 2015.

[12] Y. Pei *et al.*, "Large eddy simulation of a reacting spray flame with multiple realizations under compression ignition engine conditions," *Combust. Flame*, vol. 000, pp. 1–14, 2015.

[13] M. Jangi, R. Solsjo, B. Johansson, and X. Bai, "International Journal of Heat and Fluid Flow On large eddy simulation of diesel spray for internal combustion engines," *Int. J. HEAT FLUID FLOW*, vol. 53, pp. 68–80, 2015.

[14] L. Hakim, G. Lacaze, and J. Oefelein, "Large Eddy Simulation of Autoignition Transients in a Model Diesel Injector Configuration," 2016.

[15] G. Lacaze, A. Misdariis, A. Ruiz, and J. C. Oefelein, "Analysis of high-pressure Diesel fuel injection processes using LES with real-fluid thermodynamics and transport," *Proc. Combust. Inst.*, 2015.

[16] J. Matheis and S. Hickel, "Multi-component vapor-liquid equilibrium model for LES of high-pressure fuel injection and application to ECN Spray A," *Int. J. Multiph. Flow*, vol. 99, pp. 294–311, 2017.

[17] J. Matheis and S. Hickel, "Multi-component vapor-liquid equilibrium model for LES and application to ECN Spray A," *arXiv Prepr. arXiv1609.08533*, 2016.

[18] C. Rodriguez, P. Koukouvinis, and M. Gavaises, "Simulation of supercritical diesel jets using the PC-SAFT EoS," *J. Supercrit. Fluids*, vol. 145, pp. 48–65, Mar. 2019.

[19] C. Rodriguez, A. Vidal, P. Koukouvinis, M. Gavaises, and M. A. McHugh, "Simulation of transcritical fluid jets using the PC-SAFT EoS," *J. Comput. Phys.*, vol. 374, pp. 444–468, Dec. 2018.

[20] S.-K. Kim, H.-S. Choi, and Y. Kim, "Thermodynamic modeling based on a generalized cubic equation of state for kerosene/LOx rocket combustion," *Combust. Flame*, vol. 159, no. 3, pp. 1351–1365, 2012.

[21] M. S. Wertheim, "Fluids with highly directional attractive forces. I. Statistical thermodynamics," *J. Stat. Phys.*, vol. 35, no. 1–2, pp. 19–34, Apr. 1984.

[22] M. S. Wertheim, “Fluids with highly directional attractive forces. II. Thermodynamic perturbation theory and integral equations,” *J. Stat. Phys.*, vol. 35, no. 1–2, pp. 35–47, Apr. 1984.

[23] M. S. Wertheim, “Fluids with highly directional attractive forces. III. Multiple attraction sites,” *J. Stat. Phys.*, vol. 42, no. 3–4, pp. 459–476, 1986.

[24] M. S. Wertheim, “Fluids with Highly Directional Attractive Forces . IV . Equilibrium Polymerization,” vol. 42, pp. 477–492, 1986.

[25] W. G. Chapman, K. E. Gubbins, G. Jackson, and M. Radosz, “SAFT: Equation-of-state solution model for associating fluids,” *Fluid Phase Equilib.*, vol. 52, no. C, pp. 31–38, Dec. 1989.

[26] W. G. Chapman, G. Jackson, and K. E. Gubbins, “Phase equilibria of associating fluids,” *Mol. Phys.*, vol. 65, no. 5, pp. 1057–1079, Dec. 1988.

[27] N. Khare Prasad, “Predictive Modeling of Metal-Catalyzed Polyolefin Processes,” 2003.

[28] S. Leekumjorn and K. Krejbjerg, “Phase behavior of reservoir fluids: Comparisons of PC-SAFT and cubic EOS simulations,” *Fluid Phase Equilib.*, vol. 359, pp. 17–23, 2013.

[29] A. J. de Villiers, C. E. Schwarz, A. J. Burger, and G. M. Kontogeorgis, “Evaluation of the PC-SAFT, SAFT and CPA equations of state in predicting derivative properties of selected non-polar and hydrogen-bonding compounds,” *Fluid Phase Equilib.*, vol. 338, pp. 1–15, 2013.

[30] M. Salimi and A. Bahramian, “The prediction of the speed of sound in hydrocarbon liquids and gases: The Peng-Robinson equation of state versus SAFT-BACK,” *Pet. Sci. Technol.*, vol. 32, no. 4, pp. 409–417, 2014.

[31] K. S. Pedersen and C. H. Sørensen, “PC-SAFT Equation of State Applied to Petroleum Reservoir Fluids,” *SPE Annu. Tech. Conf. Exhib.*, vol. 1, no. 4, pp. 1–10, 2007.

[32] P. C. Ma, L. Bravo, and M. Ihme, “Supercritical and transcritical real-fluid mixing in diesel engine applications,” 2014, pp. 99–108.

[33] P. C. Ma, Y. Lv, and M. Ihme, “An entropy-stable hybrid scheme for simulations of transcritical real-fluid flows,” *J. Comput. Phys.*, vol. 340, no. March, pp. 330–357, 2017.

[34] P. C. Ma, Y. Lv, and M. Ihme, “Numerical methods to prevent pressure oscillations in transcritical flows,” no. 1999, pp. 1–12, 2017.

[35] R. W. Houim and K. K. Kuo, “A low-dissipation and time-accurate method for compressible multi-component flow with variable specific heat ratios,” *J. Comput. Phys.*, vol. 230, no. 23, pp. 8527–8553, 2011.

[36] E. F. Toro, *Reimann Solvers and Numerical Methods for fluid dynamics*, vol. 40, no. 6. 2001.

[37] T. H. Chung, M. Ajlan, L. L. Lee, and K. E. Starling, “Generalized multiparameter correlation for nonpolar and polar fluid transport properties,” *Ind. Eng. Chem. Res.*, vol. 27, no. 4, pp. 671–679, Apr. 1988.

[38] D. N. Justo-garcía, B. E. García-flores, and F. García-s, “Vapor - Liquid Equilibrium Data for the Nitrogen þ Dodecane System at Temperatures from (344 to 593) K and at Pressures up to 60 MPa,” pp. 1555–1564, 2011.

[39] C. J. Mueller *et al.*, “Diesel Surrogate Fuels for Engine Testing and Chemical-Kinetic Modeling: Compositions and Properties,” *Energy and Fuels*, vol. 30, no. 2, pp. 1445–1461, 2016.

[40] A. Vidal, C. Rodriguez, P. Koukouvinis, M. Gavaises, and M. A. Mchugh, “Modelling of Diesel fuel properties through its surrogates using Perturbed-Chain, Statistical Associating Fluid Theory.”

[41] H. B. Rokni, A. Gupta, J. D. Moore, M. A. McHugh, B. A. Bamgbade, and M. Gavaises, “Purely predictive method for density, compressibility, and expansivity for hydrocarbon mixtures and diesel and jet fuels up to high temperatures and pressures,” *Fuel*, vol. 236, no. August 2018, pp. 1377–1390, 2019.

[42] A. Tihic, G. M. Kontogeorgis, N. Von Solms, and M. L. Michelsen, “A predictive group-contribution simplified PC-SAFT equation of state: Application to polymer systems,” *Ind. Eng. Chem. Res.*, 2008.

[43] R. K. Sinnott, *Coulson & Richardson's Chemical Enginering: Volume 6/Chemical Engineering Design*. Elsevier Butterworth Heinemann, 1999.
[44] M. L. Michelsen and J. Mollerup, *Thermodynamic Modelling: Fundamentals and Computational Aspects*. Tie-Line Publications, 2004.
[45] M. L. Michelsen, "THE ISOTHERMAL FLASH PROBLEM. PART I. STABILITY," *Fluid Phase Equilib.*, vol. 9, 1982.
[46] H. Hoteit and A. Firoozabadi, "Simple phase stability-testing algorithm in the reduction method," *AIChE J.*, 2006.
[47] N. Kyriazis, P. Koukouvinis, and M. Gavaises, "Numerical investigation of bubble dynamics using tabulated data," *Int. J. Multiph. Flow*, vol. 93, no. Supplement C, pp. 158–177, 2017.
[48] S. Kawai and H. Terashima, "A high-resolution scheme for compressible multicomponent flows with shock waves," *Int. J. Numer. Methods Fluids*, vol. 66, no. 10, pp. 1207–1225, Aug. 2011.
[49] H. Terashima and M. Koshi, "Approach for simulating gas-liquid-like flows under supercritical pressures using a high-order central differencing scheme," *J. Comput. Phys.*, vol. 231, no. 20, pp. 6907–6923, 2012.
[50] H. Terashima and M. Koshi, "Corrigendum to 'Approach for simulating gas-liquid-like flows under supercritical pressures using a high-order central differencing scheme' [J. Comput. Phys., 231, 20, (2012), 6907-6923]Doi: 10.1016/j.jcp.2012.06.021," *J. Comput. Phys.*, vol. 283, pp. 609–610, 2015.
[51] P. C. Ma, H. Wu, D. T. Banuti, and M. Ihme, "On the numerical behavior of diffuse-interface methods for transcritical real-fluids simulations," *Int. J. Multiph. Flow*, pp. 231–249, Apr. 2019.
[52] B. E. Poling, J. M. Prausnitz, J. P. O'connell, and others, *The properties of gases and liquids*, vol. 5. Mcgraw-hill New York, 2001.
[53] J. Gross and G. Sadowski, "Perturbed-Chain SAFT: An Equation of State Based on a Perturbation Theory for Chain Molecules," *Ind. Eng. Chem. Res.*, vol. 40, no. 4, pp. 1244–1260, 2001.
[54] M. Farzaneh-Gord, M. Roozbahani, H. R. Rahbari, and S. J. Haghighat Hosseini, "Modeling thermodynamic properties of natural gas mixtures using perturbed-chain statistical associating fluid theory," *Russ. J. Appl. Chem.*, vol. 86, no. 6, pp. 867–878, 2013.
[55] N. Diamantonis and I. Economou, "Evaluation of SAFT and PC-SAFT EoS for the calculation of thermodynamic derivative properties of fluids related to carbon capture and sequestration," no. June 2011, pp. 1–32, 2011.
[56] B. E. Poling, *The properties of gases and liquids / Bruce E. Poling, John M. Praausnitz, John P. O'Connell*. 2001.
[57] R. Privat, R. Gani, and J. N. Jaubert, "Are safe results obtained when the PC-SAFT equation of state is applied to ordinary pure chemicals?," *Fluid Phase Equilib.*, vol. 295, no. 1, pp. 76–92, 2010.
[58] E. Scientific, P. Company, and L. Michelsen, "The isothermal flash problem. part ii. phase-split calculation," vol. 9, 1982.